Thioamide Hydroxypyrothiones Supersede Amide Hydroxypyrothiones in Potency against Anthrax Lethal Factor

Arpita Agrawal,[†] César Augusto F. de Oliveira,[†,‡] Yuhui Cheng,[†,‡] Jennifer A. Jacobsen,[†] J. Andrew McCammon,[†,‡] and Seth M. Cohen*[,†]

Department of Chemistry and Biochemistry, Howard Hughes Medical Institute, Center for Theoretical Biological Physics, and Department of Pharmacology, University of California, San Diego, 9500 Gilman Drive, La Jolla, California 92093

Received October 18, 2008

Anthrax lethal factor (LF) is a critical virulence factor in the pathogenesis of anthrax. A structure−activity relationship (SAR) of potential lethal factor inhibitors (LFi) is presented in which the zinc-binding group (ZBG), linker, and backbone moieties for a series of hydroxypyrone-based compounds were systematically varied. It was found that hydroxypyrothione ZBGs generate more potent inhibitors than hydroxypyrone ZBGs. Furthermore, coupling the hydroxypyrothione to a backbone group via a thioamide bond improves potency when compared to an amide linker. QM/MM studies show that the thioamide bond in these inhibitors allows for the formation of two additional hydrogen bonds with the protein active site. In both types of hydroxypyrothione compounds, ligand efficiencies of 0.29−0.54 kcal mol^{-1} per heavy atom were achieved. The results highlight the need for a better understanding to optimize the interplay between the ZBG, linker, and backbone to get improved LFi.

Introduction

Anthrax is one of the oldest documented diseases on record known to infect animals and to this day poses a serious threat to both animals and humans.[1] Anthrax is caused by the Gram-positive, rod-shaped bacterium *Bacillus anthracis* that is notorious for its ability to form endospores. The bacteria adopt a dormant spore structure when threatened by external factors and can survive for decades in this state before entering a host. *B. anthracis* spores are mostly soil-borne, and their dormant longevity in the soil significantly contributes to their lethality. Anthrax spores are hence among the most worrisome biological weapons used, with recent attacks in the U.S. in 2001 sparking significant concern.[2−4]

Anthrax infection can occur via three routes: inhalational, gastrointestinal, and subcutaneous, with inhalational being the most fatal. When *B. anthracis* spores are inhaled, they bind to alveolar macrophages, which phagocytose the spores and traffic them to regional lymph nodes. En route, the spores germinate to pathogenic bacteria that release a potent anthrax toxin.[5] Anthrax toxin is composed of three proteins: protective antigen (PA, 83 kDa), edema factor (EF, 89 kDa), and lethal factor (LF, 90 kDa).[a] Independently the proteins are nontoxic but in concert can induce cell death. PA first binds to one of two ubiquitous receptors, ANTXR1 (tumor endothelium marker 8) or ANTXR2 (capillary morphogenesis protein 2).[6,7] Once bound, PA is activated by the cleavage of a 20 kDa N-terminal fragment by membrane bound furin-like proteases. Upon activation, the 63 kDa PA oligomerizes to form a heptameric prepore to which three molecules of LF and/or EF can bind.[8] The complex then undergoes receptor mediated endocytosis, and the low pH in the endosome triggers a conformational change that converts the prepore to a mature cation-specific pore. LF and EF are translocated across the mature pore to the cytosol of the cell where they exert their toxicity.[9−14] EF is a calcium and calmodulin dependent adenylate cyclase that causes elevated levels of cAMP in the cytosol of infected cells and also plays a role in impairment of the immune system. Together with PA, EF forms the edema toxin (ETx).[15,16] LF is a zinc-dependent hydrolytic metalloenzyme that cleaves the N-terminus of mitogen activated protein kinase kinases (MAPKKs) to disrupt downstream signaling pathways and cause macrophage apoptosis. In combination with PA, LF forms the lethal toxin (LeTx).[15,17−19] There are several published reviews describing the pathogenesis of anthrax via its toxins, and despite extensive research in the field, the exact pathway via which LF imparts toxicity is still somewhat unclear; nevertheless, this protein is an important target for inhibition.[19−22] Current therapies against *B. anthracis* include FDA approved antibiotics such as ciproflaxin that target the bacteria but are ineffective toward the toxins secreted by the bacterium. Inactivation of the LF gene in *B. anthracis* leads to a 1000-fold reduction in its virulence, which suggests that anthrax pathology is largely dictated by LF.[22]

Several groups have been successful in developing potent lethal factor inhibitors (LFi), some of which include known matrix metalloproteinase inhibitors (MMPi).[23−34] To date, some of the most potent LFi carry a chelating hydroxamic acid zinc-binding group (ZBG) similar to other zinc metalloprotease inhibitors. Hydroxamic acids are known to be limited by poor oral availability, limited zinc(II) ion selectivity, and poor pharmacokinetics.[35,36] To overcome the limitations of hydroxamic acids, the design of LFi that incorporate alternative ZBGs merits investigation.

In this study we have focused on a three component strategy to the design of an LFi: (i) a ZBG to chelate and inactivate the catalytic Zn^{2+} ion, (ii) a backbone to interact noncovalently with the LF active site, and (iii) a linker to connect the backbone to

* To whom correspondence should be addressed. Telephone: (858) 822-5596. Fax: (858) 822-5598. E-mail: scohen@ucsd.edu.

† Department of Chemistry and Biochemistry.

‡ Howard Hughes Medical Institute, Center for Theoretical Biological Physics, and Department of Pharmacology.

[a] Abbreviations: LF, lethal factor; LeTx, lethal toxin; EF, edema factor; ETx, edema toxin; PA, protective antigen; AHA, acetohydroxamic acid; LFi, lethal factor inhibitor(s); ZBG, zinc binding group; QM/MM, quantum mechanics/molecular mechanics; LE, ligand efficiency; BPCA, 3-(benzyloxy)-4-oxo-4*H*-pyran-2-carboxylic acid; BDCA, 1-(benzyloxy)-6-oxo-1,6-dihydropyridine-2-carboxylic acid.

10.1021/jm8013212 CCC: $40.75
Published on Web 01/26/2009

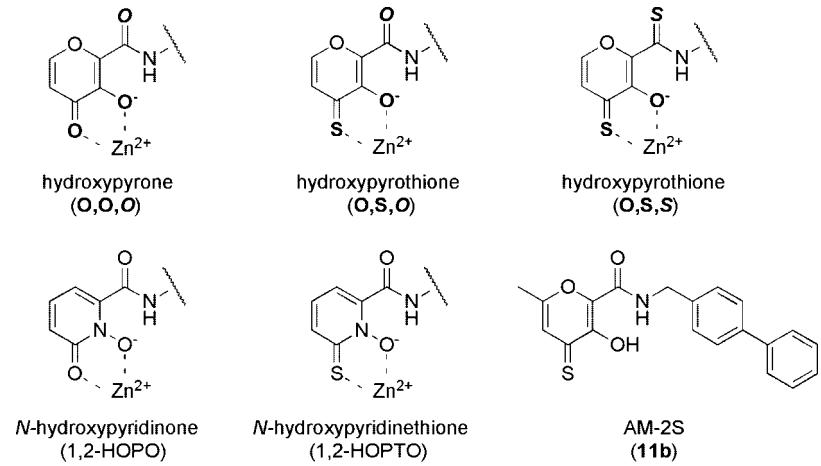

Figure 1. ZBGs and linkers used in the LFi reported here. Abbreviations for each subset of compounds are shown in parentheses. The heteroatom terminology used throughout is highlighted in the top three structures by the use of bold and italics atom labels. Shown in the bottom right is the complete LFi **11b**.

the ZBG. A similar overall scheme has been used in the development of MMP and histone deacetylase (HDAC) inhibitors.[37,38] In the work presented here, the specific ZBGs employed are derivatives of 3-hydroxy-2-methyl-4-pyrone (maltol), 3-hydroxy-2-methyl-4-pyrothione (thiomaltol), 1-hydroxypyridin-2(1*H*)-one (1,2-HOPO), and 1-hydroxypyridine-2(1*H*)-thione (1,2-HOPTO). We have shown that these compounds are effective ZBGs for inhibiting LF and other metalloproteinases.[39−44] The study presented here is focused on the synthesis and structure−activity relationship (SAR) of the hydroxypyrone- and hydroxypyrothione-based LFi. Different aromatic backbones were attached to the ZBGs via an amide or a thioamide linkage. The results presented elucidate the contribution of each component to the potency of the different LFi. The potency of each inhibitor was tested in vitro by using a fluorescence-based assay that has been previously reported.[40,45] The potency of each LFi is reflected in calculated kinetic parameters such as IC_{50}, K_i, and ligand efficiency. In order to better understand the importance of the linker and backbone in protein−inhibitor interactions, computational studies were performed to build three-dimensional models of the inhibitors bound to the LF active site. Our computational models are in agreement with the experimental results and suggest a key role of the thioamide group in stabilizing the protein−inhibitor complex.

Results

Synthesis of LFi. Our group has previously identified alternative ZBGs that are more potent than simple hydroxamic acids against LF.[39,40] On the basis of these earlier findings, a novel hydroxypyrothione-based (O,S metal-binding donor atom set) LFi (AM-2S, **11b**, Figure 1) was designed, synthesized, and found to be moderately potent against LF (IC_{50} = 13.9 μM).[40] **11b** thereby inspired the design of additional hydroxypyrone, hydroxypyrothione, *N*-hydroxypyridinone, and *N*-hydroxypyridinethione LFi shown in Figures 1 and 2. Compounds **1a** (PY-2) and **9a** (1,2-HOPO-2) were previously synthesized and identified as potent nanomolar inhibitors against deep pocket MMPs.[46] Several similar compounds comprising hydroxypyrone ZBGs (O,O metal-binding donor atom set), amide linking groups, and a series of different backbone substituents were synthesized (Scheme 1, Figure 2, **1a**−**10a**).[46] Compounds **1a**−**10a** were universally found to be ineffective as LFi (vide supra).

Because compounds **1a**−**10a** were not potent LFi and our previously reported inhibitor (**11b**) used a hydroxypyrothione ZBG, compounds **1a**−**10a** were similarly converted to their O,S donor hydroxypyrothione analogues. Reaction of the hydroxypyrone compounds **1a**−**10a** with phosphorus pentasulfide (P_4S_{10}) and hexamethyldisiloxane (HMDO) in benzene generates two products as shown in Scheme 2. One major product contains a single sulfur atom, designated (O,S,*O*) compounds, at the pyrone carbonyl group. The second major product contains two sulfur atoms, designated (O,S,*S*) compounds, with one sulfur atom at the pyrone carbonyl group and the other at the amide carbonyl linker group. This structural assignment was based on the spectroscopic characterization of the compounds (^{1}H NMR and ^{13}C NMR) and was unambiguously confirmed by an X-ray crystal structure of compound **5c** (vide infra).

Upon thionation of the hydroxypyrone (O,O,*O*) compounds, the (O,S,*O*) compounds are produced first followed by production of the (O,S,*S*) compounds. The pyrone carbonyl oxygen of each compound reacts prior to conversion of the amide to a thioamide linker, and therefore, the percentage of each major product can be modulated by the reaction time. However, the reactivity of each compound was found to also depend on the backbone substituent. When **1a**, with a biphenyl backbone, was treated with P_4S_{10} and HMDO for 3 h, the reaction yielded **1b** (O,S,*O*) in 16% and **1c** (O,S,*S*) in 43% yield, respectively. When **1a** was treated for about 1 h, **1b** and **1c** were obtained in 69% and 2% yields, respectively. When **8a**, with a simple ethyl backbone was treated for only 30 min, the isolated products consisted of 55% **8b** (O,S,*O*) and 20% **8c** (O,S,*S*). Similarly, when the reaction time was extended to 1 h, **8b** was obtained in 25% yield, whereas **8c** was isolated in a 43% yield. The results obtained show that optimal reaction times have to be considered for each compound of interest. An additional point of interest is that the R_f values for the (O,S,*O*) and (O,S,*S*) compounds tend to be very similar and chromatographic separation can be challenging (hence, the poor to moderate yields reported here).

As for the *N*-hydroxypyridinone-based (1,2-HOPO) inhibitors, synthesis of **9a** was previously reported;[46] the synthesis of **10a** parallels the synthetic procedure for **9a** (Scheme 3). Unlike the hydroxypyrothiones described above, the syntheses of the *N*-hydroxypyridinethione-based (1,2-HOPTO) inhibitors are not derived from their O,O chelate analogues. The synthesis of 1-hydroxy-6-thioxo-1,6-dihydropyridine-2-carboxylic acid (HTDCA) in Scheme 4 is based on literature procedures with slight modifications (see Experimental Section).[47,48] Syntheses of **9b** and **10b** from HTDCA are outlined in Scheme 4. The 4-phe-

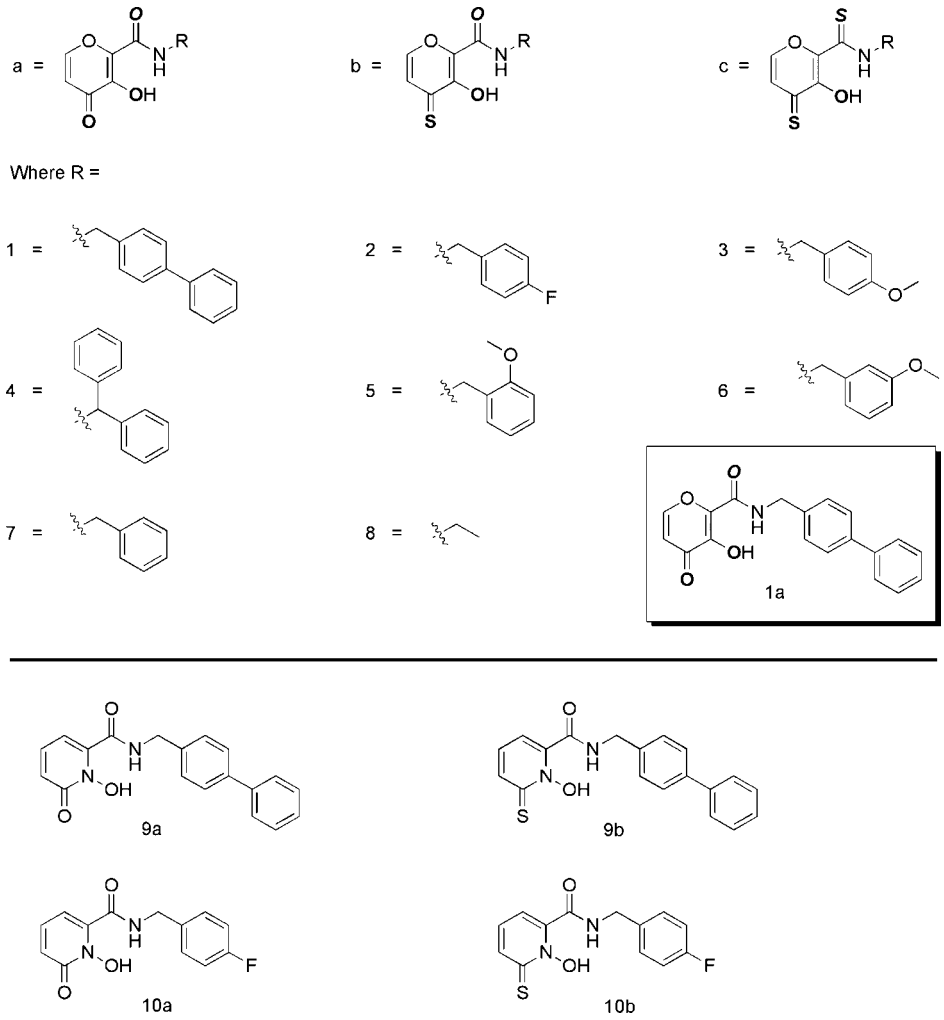

Figure 2. Structures of the inhibitors tested in this study. The heteroatom terminology used throughout is highlighted in the top three structures by the use of bold and italics atom labels. Shown in the box is the complete LFi **1a** (for clarity). Other inhibitors are hydroxypyrones with an amide linker (**1a**−**8a**), hydroxypyrothiones with an amide linker (**1b**−**8b**), hydroxypyrothiones with a thioamide linker (**1c**−**8c**), *N*-hydroxypyridinones with an amide linker (**9a**, **10a**, below thick line), and *N*-hydroxypyridinethiones with an amide linker (**9b**, **10b** below thick line).

nylbenzylamine and 4-fluorobenzylamine backbones are appended to HTDCA under standard amide coupling conditions. EDCI (1-ethyl-3-(3-dimethylaminopropyl) carbodiimide) and NHS (*N*-hydroxysuccinimide) were used as the coupling reagents for **9b**, whereas EDCI and HOBt (*N*-hydroxybenzotriazole) were the coupling reagents used in the production of **10b**.

Single-Crystal X-ray Structure of 5c. To provide evidence for the conversion of both carbonyl oxygen atoms to sulfur, an X-ray diffraction study was performed on inhibitor **5c**. Large red plates of **5c** were obtained by slow evaporation from a concentrated solution of the compound in chloroform. The crystal structure (Figure S1 and Table S2 of Supporting Information) confirms the presence of the two expected sulfur atoms. In addition to the measured electron density, the C−S bond lengths confirm the correct identity of the sulfur atoms. The thionyl C(4)−S(4) bond distance of 1.66 Å lies within the range of C−S bonds from other hydroxypyrothiones (1.68 Å).[42] The thioamide C(1)−S(1) bond distance of 1.68 Å is similar to the average thioamide bond distance (1.67 Å) predicted from the Cambridge Crystallographic Data Center (CCDC) and is too long to be an amide C−O bond (∼1.22 Å).

In Vitro Potency. The in vitro potency of each inhibitor was evaluated against LF using an established procedure with a quenched fluorogenic substrate, where observed fluorescence is directly proportional to LF activity.[45] The IC_{50} values (Table 1) were calculated for each synthesized inhibitor as described under Experimental Section. Kinetic parameters (V_{max}, K_m, K_i) were also calculated using the same fluorogenic assay. Additionally, ligand efficiencies of most inhibitors were calculated from the respective K_i values (vide infra).[49−51] Compounds **1a**−**8a** (Table 1, column "**a**"), which consist of a hydroxypyrone ZBG and amide linker (O,O,*O*), are ineffective against LF with IC_{50} values greater than 100 μM. Compounds **1b**−**8b** (Table 1, column "**b**"), which consist of a hydroxypyrothione ZBG and amide linker (O,S,*O*), show moderate potency against LF with IC_{50} values ranging from 13 to >100 μM. Surprisingly, compounds **1c**−**8c** (Table 1, column "**c**"), which consist of a hydroxypyrothione ZBG and thioamide linker (O,S,*S*), are uniformly the most potent compounds with IC_{50} values in the range 5−11 μM. Together these data show that (i) a hydroxypyrone ZBG when coupled via an amide linker (O,O,*O*) is ineffective against LF regardless of the backbone used, (ii) a hydroxypyrothione ZBG when coupled via an amide linker (O,S,*O*) can have moderate potency against LF depending on the backbone substituent, and (iii) a hydroxypyrothione ZBG when coupled via a thioamide linker (O,S,*S*) provides consistent potency against LF with little influence from the backbone group. The minimal effect of the backbone in compounds **1c**−**8c** is highlighted by inhibitor **8c**, which utilizes only a simple ethyl

Scheme 1. Synthesis of Hydroxypyrone (O,O,*O*) Inhibitors (**1a**−**8a**)[a]

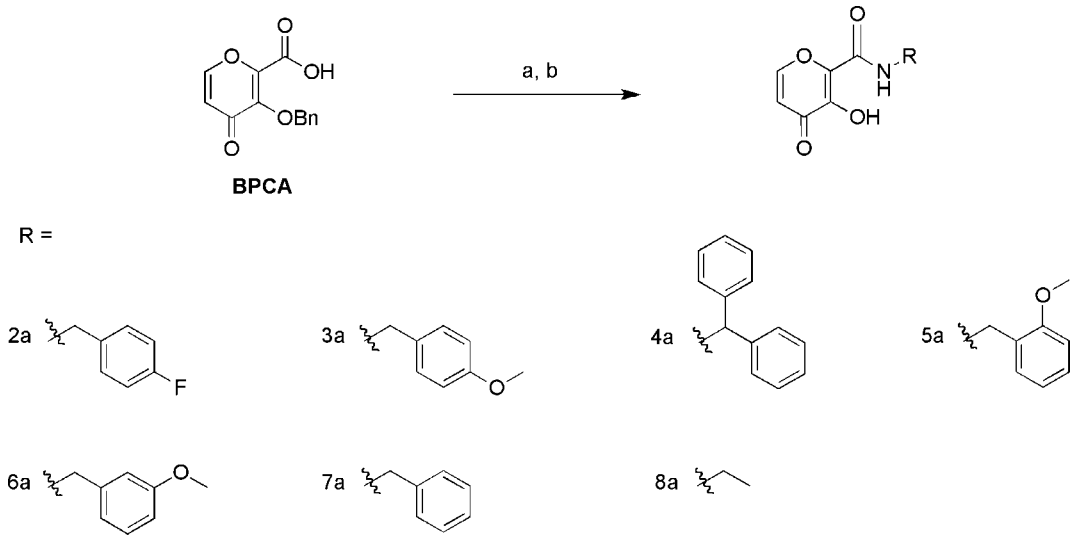

[a] Reagents and conditions: (a) RNH_2, EDCI, HOBt, CH_2Cl_2, N_2, room temp; (b) 1:1 HCl/CH_3COOH, room temp.

Scheme 2. Synthesis of Hydroxypyrothione Analogues **1b** (O,S,*O*) and **1c** (O,S,*S*) Compounds[a]

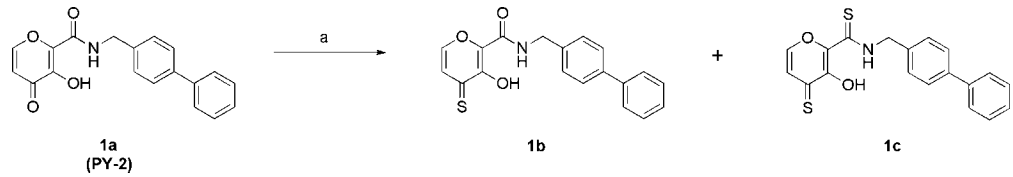

[a] Reagents and conditions: (a) P_4S_{10}, HMDO, benzene, 110 °C.

Scheme 3. Synthesis of *N*-Hydroxypyridinone **10a**[a]

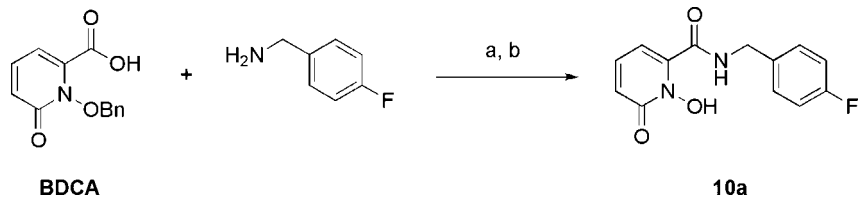

[a] Reagents and conditions: (a) EDCI, HOBt, CH_2Cl_2, N_2, room temp; (b) 1:1 HCl/CH_3COOH, room temp, 32%.

backbone and yet has a similar IC_{50} value compared to the rest of the series that employ a variety of aromatic backbones. These findings thus underline the importance of all three components, the ZBG, linker, and backbone, and that each of these components must be considered when optimizing LFi.

In order to confirm the importance of the ZBG and linker in generating effective LFi, we synthesized four additional inhibitors, based on *N*-hydroxypyridinone (**9a**, **10a**) and *N*-hydroxypyridinethione (**9b**, **10b**) chelators. Compounds **9a** and **9b** contain the same biphenyl backbone and amide linker found in **1a**. Compounds **10a** and **10b** have the same fluorobenzyl backbone and amide linker as compound **2a**. Therefore, on the basis of our earlier classification, **9a** and **10a** are (O,O,*O*) inhibitors like **1a** and **2a**; **9b** and **10b** are (O,S,*O*) inhibitors similar to **1b** and **2b**. Notably, the only difference between these inhibitors lies in the use of a *N*-hydroxypyridinone (1,2-HOPO) versus hydroxypyrone, or *N*-hydroxypyridinethione (1,2-HOPTO) versus hydroxypyrothione ZBG. These heterocyclic ZBGs are essentially isosteric and very similar in overall composition. With that in mind, it was surprising to find that whereas the (O,O,*O*) hydroxypyrones (**1a**, **2a**) are less effective than the (O,S,*O*) hydroxypyrothiones (**1b**, **2b**), no substantial differences are seen between the 1,2-HOPO (**9a**, **10a**) and 1,2-HOPTO (**9b**, **10b**) compounds, with the latter inhibitors showing very poor potency (>100 μM). The lack of potency of the 1,2-HOPO and 1,2-HOPTO chelators may be due to (a) a significantly different binding mode of these chelators to the active site zinc(II) ion or (b) the significantly greater acidity of these chelators relative to the hydroxypyrones and hydroxypyrothiones. In either case, this data show that the nature of the ZBG is critical and that even small changes in structure can result in large differences in efficacy.

Computational Modeling. In order to verify the structural and energetic factors that are relevant for the differences in observed potency, we built QM/MM optimized structures for the bound complex between the LF active site and several of the hydroxypyrothione inhibitors. Figure 3 displays the models for the bound structures of inhibitors **1b**, **1c**, **3b**, **3c**, **4b**, and **4c** in the active site of LF. Interestingly, optimized structures of molecules **1b** and **1c** in the active site of LF presented very similar configurations and no significant difference was observed in the orientation of the backbone fragment or the amide and thioamide linker groups. This is consistent with the observations that **1b** and **1c** have similar IC_{50} values against LF. In contrast,

Scheme 4. Synthesis of *N*-Hydroxypyridinethione Inhibitors **9b** and **10b**[a]

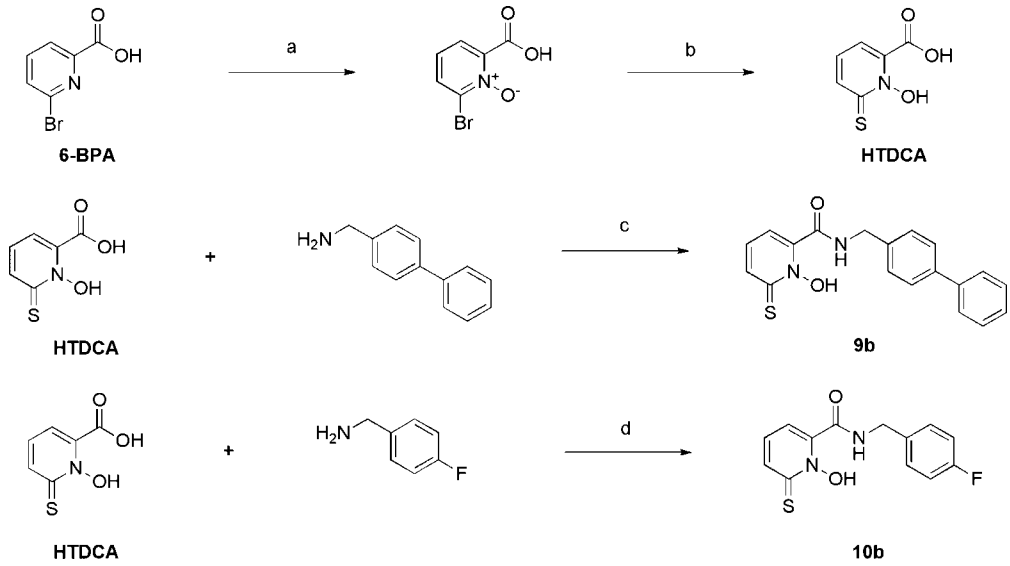

[a] Reagents and conditions: (a) TFA, 30% H_2O_2, 80 °C, 94%; (b) Na^+HS^-, H^+Cl^-, 95 °C, 89%; (c) EDCI, NHS, CH_2Cl_2, 46%; (d) EDCI, HOBt, CH_2Cl_2, 95%.

Table 1. IC_{50} Values of LFi Using a Fluorescence-Based Assay[a]

	IC_{50} (μM)		
compd	**a** (O,O,*O*)	**b** (O,S,*O*)	**c** (O,S,*S*)
1	>100	13.2 (±0.9)	8.3 (±0.1)
2	>100	29.2 (±1.4)	9.2 (±0.2)
3	>100	50.4 (±2.4)	10.6 (±0.6)
4	>100	14.1 (±2.0)	5.0 (±0.2)
5	>100	33.5 (±2.3)	8.7 (±0.8)
6	>100	37.4 (±3.1)	6.6 (±0.8)
7	>100	>100	7.9 (±0.6)
8	>100	72.5 (±5.4)	11.4 (±0.7)
9	>100	>50[b]	
10	>100	>100	

[a] All values represent the average and standard deviation from at least three independent experiments. [b] Determination of a more accurate IC_{50} value was precluded by the limited solubility of this compound.

even though the backbone fragments of **3b** and **3c** adopt similar configurations, the ZBG relative to the amide/thioamide linker groups shows distinct orientations. By comparing the structures of **1c** and **3c**, we observed that the sulfur atom of the thioamide group acts as a hydrogen bond acceptor, interacting with the backbone amide *N*-H group of residues Lys392 and Gly393. Similar hydrogen bonding was also observed in the optimized structures of thioamide containing LFi: **2c**, **7c**, and **8c** (Figure S3). Figure 3 shows that although the two hydrogen bonds were observed in the complexes of LF with **1b**, **1c**, and **3c**, they were not found with compound **3b**. The distance between the amide oxygen of **3b** and the backbone *N*-H groups was greater than 4.0 Å (Figure 3). These observations are consistent with the IC_{50} values obtained for these compounds (Table 1), where **3b** is clearly the least effective of these inhibitors (50.4 μM). Similar interactions involving either Lys392 or Gly393 have already been characterized in crystal structures of anthrax lethal factor bound to small molecule inhibitors, which indicate that these residues may play an important role in the inhibitor binding.[32,33]

Previous work suggested that the plasticity and flexibility of the S1′ binding pocket allow the receptor to accommodate small and large hydrophobic residues at the P1′ position.[33] These studies also indicate that the design of compounds with greater complementarity to the S1′ pocket would lead to potent and selective inhibition of LF. In order to explore interactions with the S1′ binding pocket, inhibitors **4b** and **4c** were designed. In fact, **4c** shows a modest, ~2-fold improvement in LF potency when compared to **1c**.

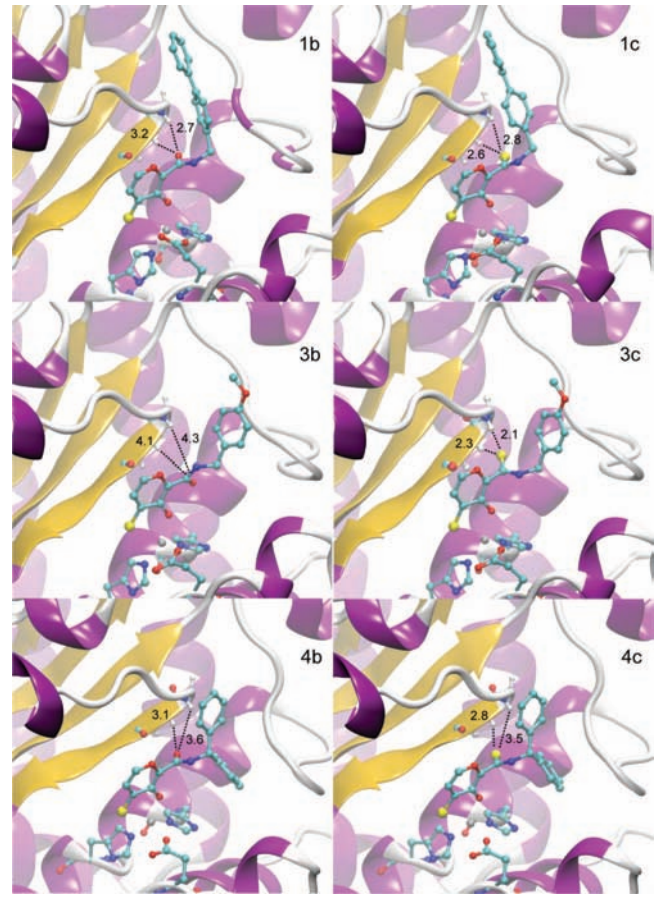

Figure 3. QM/MM optimized structures of the complex between anthrax LF (ribbons) and inhibitors **1b**, **1c**, **3b**, **3c**, **4b**, and **4c** (ball-and-stick). Some active site residues (ball-and-stick) and catalytic zinc(II) ion (gray sphere) are also shown.

To further investigate the quality of our models, all optimized structures were submitted to energy calculation procedures by

using the program Autodock 4.0.[52] Because there is a good agreement between the calculated structures and the experimentally determined IC_{50} values, the calculated models were used to obtain a rough estimation of the binding free energy of molecules **1b**, **1c**, **2b**, **2c**, **3b**, **3c**, **4b**, and **4c**. Figure S2 of Supporting Information shows the plot of log(IC_{50}) value against the estimated free energy of binding (ΔG), which demonstrates that the trend in potency is captured reasonably well by the calculated models.

Discussion

Anthrax lethal factor is a zinc dependent endopeptidase that cleaves MAPKKs 1−4, 6, and 7 to inhibit downstream pathways that culminate in macrophage apoptosis. The Zn^{2+} ion in the lethal factor active site is tetrahedrally coordinated via two histidine residues (His686 and His690), one glutamic acid residue (Glu735), and one water molecule. The bound water molecule in this motif, which occurs in several different zinc metalloproteases, is responsible for substrate cleavage.[53] Our goal is to exploit the presence of a metal ion and develop LFi that can chelate and inactivate the catalytic zinc(II) ion while optimizing the noncovalent interactions of the backbone component with the protein active site. Most LFi and metalloprotein inhibitors in the literature utilize a hydroxamic acid as the ZBG; however, the poor pharmacokinetics of hydroxamates has made the search for alternative chelators a prudent topic of interest.[39,43]

Of the previously reported ZBGs, hydroxypyrothiones were determined to be the most potent against LF and thus were incorporated into the LFi **11b** as shown in Figure 1.[40] **11b** inspired the design of additional hydroxypyrothione inhibitors as shown in Figure 2, along with their hydroxypyrone precursors, to develop a structure−activity-relationship (SAR). The overall goal was to design and synthesize different inhibitors with variations in three key components (the ZBG, linker, and backbone) and to analyze the contribution of each component toward potency against LF.

Figure 2 shows the compounds that were synthesized for this study which also include MMPi (**1a** and **9a**) that were previously reported.[46] As shown in Figure 2, four different ZBGs (hydroxypyrone, hydroxypyrothione, *N*-hydroxypyridinone, *N*-hydroxypyridinethione), two different linkers (amide and thioamide), and eight different backbones were assembled in different combinations to generate 28 compounds. Table 1 lists the IC_{50} values of each compound against LF. As previously noted, the *N*-hydroxypyridinone- (both O,O,*O* and O,S,*O*) and the hydroxypyrone-based (O,O,*O*) compounds are poor inhibitors of LF. In contrast, the (O,S,*O*) hydroxypyrothione ZBG clearly improves inhibition of LF, consistent with the earlier studies on **11b**.[40]

A three-dimensional structure of the bound complex formed between **11b** and anthrax LF showed the biphenyl backbone of **11b** targeting a specific pocket in the LF active site.[40] To optimize the backbone interactions in LF, different substituted and unsubstituted aromatic backbones were appended to the ZBGs via an amide or thioamide linker. The hydroxypyrothiones coupled via an amide bond (O,S,*O*) showed moderate potency (consistent with **11b**) with some variations depending on the backbone group. However, the use of a thioamide linker with a hydroxypyrothione ZBG (O,S,*S*) showed consistently improved potency against LF, regardless of the backbone used. These results suggested that the potency of the (O,S,*S*) compounds was primarily a result of the ZBG and linker alone. To improve potency by enhancing backbone interactions, we targeted the S1′ pocket of LF with the design of inhibitor series **4a**−**c**. The "bifurcated" biphenyl backbone of **4c** was designed to interact with the same pocket as found for **11b** while also targeting the S1′ pocket. Compound **4c** showed a slight but not pronounced improvement in inhibition compared to the other LFi reported here. To confirm the dominance of the ZBG and linker over the backbone in this series of LFi, compounds with a simple ethyl backbone were prepared (**8a**−**c**). Indeed, the potency of **8c** showed that the backbone groups play a minimal role in these compounds, and further design is required to fully exploit additional protein-specific interactions.

To probe the specific interactions of the ZBG, linker, and backbone in the active site, computational models for the binding mode of several of the inhibitors were calculated using the previously calculated **11b** model as a starting point.[40] QM/MM minimization procedures were employed on each model in order to take into account electronic effects in the interaction between zinc(II), the active site residues, and the ZBG. The models show a good agreement, at least qualitatively, with the experimentally observed IC_{50} values. The optimized structures reveal that different backbone fragments have little effect on the orientation of the ZBG in the active site. The main structural difference found in our models was in the orientation of the amide/thioamide linker relative to the ZBG. The models show that twisting about the bond between the ZBG and the amide group (e.g., breaking planarity of the amide group and aromatic pyrone rings) allows for formation of specific interactions between residues Lys392, Gly393, and the oxygen/sulfur amide atoms of the inhibitors. Dihedral angles between the amide/thioamide groups and pyrone rings in **1b**, **1c**, **3b**, **3c**, **4b**, and **4c** were found to be 71°, 62°, 28°, 98°, 61°, and 57°, respectively. The hydrogen bonding is most pronounced in the inhibitor with bulky backbones (**1b,c** and **4b**,**c**), where the hydrogen-bonded amide/thioamide linkers sit in essentially the same configuration (Figure 3). The smaller angle in **3b** is consistent with the lack of hydrogen bonding (Figure 3) with the protein active site compared to the other LFi. It is important to note that QM minimizations of the inhibitors, in the absence of protein and solvation, converge to a planar thioamide−pyrone ring conjugated system. This was validated by minimizing the conformation of **5c**, which converged to the structure found by crystallographic analysis (Figure S1 of Supporting Information). The hydrogen bond formed by the thioamide LFi was somewhat surprising, as thioamides are known to be weaker hydrogen bond acceptors compared to their amide analogues.[54,55] However, Allen and co-workers have shown that thioamides possess a resonance induced hydrogen bonding potential that arises from the lone pair of electrons on the neighboring nitrogen atom of the amino group.[54] This leads to a net increase in electronegativity of the thioamide sulfur and a lengthening of the C═S bond, which likely facilitates hydrogen bonding in these molecules.

Despite the difference in potency among the (O,S,*O*) and (O,S,*S*) compounds, the ligand efficiencies (LE) of both sets of hydroxypyrothiones fall in a reasonably efficient, small window of 0.28−0.54 kcal mol^{-1} per heavy atom.[49−51] LE is the ratio of the binding free energy of a ligand to the number of heavy atoms in the ligand. LE is used to normalize the potency of various ligands with respect to their molecular weight.[49−51,56] In this way, LE is an important metric in controlling the size of a druggable lead while maintaining potency. The LE of the hydroxypyrothione ZBG (i.e., thiomaltol) is 0.58 kcal mol^{-1} per heavy atom and with the addition of a thioamide ethyl linkage (**8c**) is 0.54 kcal mol^{-1} per heavy atom. The remaining hydroxypyrothione LFi with aromatic backbones have an

average LE of 0.33 kcal mol^{-1} per heavy atom. The potency contributed by the thioamide bond is further reflected in the similar LE values obtained for thiomaltol and **8c** and remains relatively consistent throughout the LFi series compared to their amide analogues. As discussed above, the potency of the thioamide-linked compounds may be attributed to the longer C═S bond and twisting of the ZBG, which helps to introduce hydrogen bonding with the protein active site.[54,57]

There is some concern about the clinical use of thioamides, as in some cases they have been associated with hepatotoxic effects.[58,59] However, other studies have shown thioamides to improve the stability of compounds against certain proteases.[57,60,61] In this study, in addition to being more potent, the thioamide LFi reported here meet certain drug discovery criteria, with molecular weights of less than 500 Da, possessing less than 5 hydrogen-bond donors and less than 10 hydrogen-bond acceptors with adequate ligand efficiencies.[56] To further develop the hydroxypyrothione ZBGs with a thioamide linker, we plan to utilize our computational models to probe the active site and further elaborate the (O,S,*S*) scaffold with more specific, protein-interacting backbones.

Conclusion

In this report we have successfully shown the effect of the ZBG and linker on the potency of a series of metal-chelating LFi. Some of the compounds include potent, isoform-specific MMPi (**1a** and **9a**) that showed negligible activity against LF. The active inhibitors identified here elicit the effect by tight binding of the ZBG and strong hydrogen bonding to the protein via a thioamide linking group. Even though at present we have not identified an optimal backbone component, we have succeeded in identifying a potent ZBG−linker scaffold from which an optimized backbone can be grafted to obtain a new class of highly potent LFi.

Experimental Section

Chemistry. Unless otherwise noted, all chemicals were purchased from commercial suppliers (Aldrich and Fisher) and used as received. Flash silica gel chromatography was performed using Merck silica gel 40−63 μm mesh. Inert reactions were carried out under a dinitrogen atmosphere. $^1H/^{13}C$ NMR spectra were recorded at ambient temperature on a 300 or 400 MHz Varian FT-NMR instrument, property of the Department of Chemistry and Biochemistry, University of California, San Diego. Mass spectra were obtained at the Small Molecule Mass Spectrometry Facility in the Department of Chemistry and Biochemistry at the University of California, San Diego. Elemental analysis was performed by NuMega Resonance Laboratories, San Diego, CA.

***N*-(Biphenyl-4-ylmethyl)-3-hydroxy-4-oxo-4*H*-pyran-2-carboxamide (1a).** This compound was prepared as previously reported.[46]

***N*-(Biphenyl-4-ylmethyl)-3-hydroxy-4-thioxo-4*H*-pyran-2-carboxamide (1b).** To a solution of **1a** (200 mg, 0.62 mmol) in benzene (20 mL) was added P_4S_{10} (0.366 equiv, 102 mg, 0.23 mmol) and HMDO (3.339 equiv, 336 mg, 442 μL, 2.07mmol), and the mixture was heated to reflux at 105 °C for 3 h. Solid byproducts were removed by vacuum filtration, and the filtrate was evaporated in vacuo to a crude brown solid. The crude product was purified via column chromatography (50% EtOAc/hexanes) to afford **1b** (33 mg, 0.10 mmol). Yield = 16%. ^1H NMR (400 MHz, $CDCl_3$, 25 °C): δ = 4.71 (d, J = 6 Hz, NHCH_2), 7.34 (t, J = 7.2 Hz, 1H; ArH), 7.42 (m, 5H; ArH), 7.57 (m, 4H; ArH), 7.72 (d, J = 5.2 Hz, 1H; ArH), 7.92 (brt, 1H; CON*H*CH_2), 9.73 (brs, 1H; ArOH). ^{13}C NMR (100 MHz, $CDCl_3$, 25 °C): δ = 43.6 (CH_2), 125.7 (ArC), 127.1 (ArC), 127.4 (ArC), 127.6 (ArC), 128.3 (ArC), 128.8 (ArC), 132.4 (ArC), 136.0 (ArC), 140.5 (ArC), 140.9 (ArC), 147.4 (ArC), 151.6 (ArC), 160.9 (C═O), 190.5 (ArC═S). APCI-MS(−) *m*/*z* 336.11 $[M - H]^-$. Anal. ($C_{19}H_{15}NO_3S \cdot H_2O$). C, H, N, S, respectively: calcd 64.21, found 64.51; calcd 4.82, found 4.94; calcd 3.94, found 3.89; calcd 10.80, found 11.26.

***N*-(Biphenyl-4-ylmethyl)-3-hydroxy-4-thioxo-4*H*-pyran-2-carbothioamide (1c). 1c** was obtained from **1a** from the same reaction as that of **1b** (vide supra) as a dark-brown solid (94 mg, 0.27 mmol). Yield = 43%. ^1H NMR (400 MHz, $CDCl_3$, 25 °C): δ = 5.01 (d, J = 4.4 Hz, NHCH_2), 7.35 (t, J = 7.4 Hz, 1H; ArH), 7.42 (m, 5H; ArH), 7.58 (m, 4H; ArH), 7.75 (d, J = 5.2 Hz, 1H; ArH), 9.53 (brt, 1H; CON*H*CH_2), 10.30 (brs, 1H; ArOH). ^{13}C NMR (100 MHz, $CDCl_3$, 25 °C): δ = 50.0 (CH_2), 125.3 (ArC), 127.0 (ArC), 127.5 (ArC), 127.7 (ArC), 128.6 (ArC), 128.8 (ArC), 133.9 (ArC), 134.2 (ArC), 140.2 (ArC), 141.2 (ArC), 147.4 (ArC), 149.3 (ArC), 184.8 (C═S), 191.2 (ArC═S). APCI-MS(+) *m*/*z* 353.98 $[M + H]^+$. Anal. ($C_{19}H_{15}NO_2S_2 \cdot 0.65H_2O$). C, H, N, S, respectively: calcd 62.49, found 662.29; calcd 4.50, found 4.45; calcd 3.84, found 3.66; calcd 17.56, found 17.40.

***N*-(4-Fluorobenzyl)-3-hydroxy-4-oxo-4*H*-pyran-2-carboxamide (2a).** To a solution of 3-(benzyloxy)-4-oxo-4*H*-pyran-2-carboxylic acid (BPCA)[46] (500 mg, 2.0 mmol) in dichloromethane was added NHS (1.0 equiv, 230 mg, 2.0 mmol), EDCI (1.0 equiv, 383 mg, 2.0 mmol), and 4-fluorobenzylamine (1.0 equiv, 250 mg, 227 μL, 2.0 mmol). The mixture was stirred overnight at room temperature under N_2 and then poured into a separatory funnel and extracted with water and dichloromethane. The layers were separated, and the organic layers were combined, dried over anhydrous magnesium sulfate, filtered, and concentrated to an orange oil. The crude oil was purified via silica column chromatography (0−2% MeOH/CH_2Cl_2) to yield a yellow solid of the benzyl protected product. To the yellow product was added 10 mL of a 1:1 solution of concentrated HCl and glacial acetic acid. The reaction mixture was stirred for 5 d and then concentrated in vacuo to yield an off-white residue which was coevaporated with MeOH and dried to yield an off-white solid (269 mg, 1.02 mmol). Yield = 93%. ^1H NMR (400 MHz, $CDCl_3$, 25 °C): δ = 4.46 (d, J = 6 Hz, NHCH_2), 6.32 (d, J = 5.6 Hz, 1H; ArH), 6.90 (t, J = 8.4 Hz, 2H; ArH), 7.20 (dd, J = 3.6, 14, 2H; ArH), 7.67 (d, J = 5.2 Hz, 1H; ArH), 8.11 (brt, 1H; CON*H*CH_2). ^{13}C NMR (100 MHz, $CDCl_3$, 25 °C): δ = 42.1 (CH_2), 114.8 (ArC), 115.0 (ArC), 115.2 (ArC), 129.1 (ArC), 129.2 (ArC), 132.9 (ArC), 148.9 (ArC), 153.2 (ArC), 160.5 (ArC), 162.4 (ArC), 162.9 (C═O), 173.6 (ArC═O). ESI-MS(+) *m*/*z* 264.02 $[M + H]^+$. Anal. ($C_{13}H_{10}FNO_4$) C, H, N.

***N*-(4-Fluorobenzyl)-3-hydroxy-4-thioxo-4*H*-pyran-2-carboxamide (2b).** This compound was prepared from **2a** according to the procedure outlined for **1b**. **2a** (150 mg, 0.57 mmol) was treated with P_4S_{10} and HMDO for 1 h to yield an orange-red solid of **2b** (48 mg, 0.17 mmol). Yield = 30%. ^1H NMR (400 MHz, $CDCl_3$, 25 °C): δ = 4.63 (d, J = 6 Hz, NHCH_2), 7.02 (t, J = 9.4 Hz, 2H; ArH), 7.31 (m, 2H; ArH), 7.42 (dd, J = 3.6, 6.4 Hz, 1H; ArH), 7.72 (dd, J = 3.6, 6.4 Hz, 1H; ArH), 7.90 (brt, 1H; CON*H*CH_2), 9.65 (brs, 1H; ArOH). ^{13}C NMR (100 MHz, $CDCl_3$, 25 °C): δ = 42.5 (CH_2), 115.0 (ArC), 115.2 (ArC), 126.4 (ArC), 129.1 (ArC), 129.2 (ArC), 131.3 (ArC), 146.2 (ArC), 152.7 (ArC), 160.7 (ArC), 162.2 (ArC), 163.1 (C═O), 191.5 (ArC═S). APCI-MS(+) *m*/*z* 280.06 $[M + H]^+$. Anal. ($C_{13}H_{10}FNO_3S$) C, H, N, S.

***N*-(4-Fluorobenzyl)-3-hydroxy-4-thioxo-4*H*-pyran-2-carbothioamide (2c). 2c** was obtained from **2a** from the same reaction as that of **2b** as a brown solid (47 mg, 0.16 mmol). Yield = 28%. ^1H NMR (400 MHz, $CDCl_3$, 25 °C): δ = 4.94 (d, J = 4.8 Hz, NHCH_2), 7.06 (t, J = 8.8 Hz, 2H; ArH), 7.35 (dd, J = 2.8, 13.6 Hz, 2H; ArH), 7.41 (d, J = 5.2 Hz, 1H; ArH), 7.76 (d, J = 4.8 Hz, 1H; ArH), 9.50 (brt, 1H; CON*H*CH_2), 10.18 (brs, 1H; ArOH). ^{13}C NMR (100 MHz, $CDCl_3$, 25 °C): δ = 49.4 (CH_2), 115.8 (ArC), 116.0 (ArC), 125.2 (ArC), 129.8 (ArC), 130.0 (ArC), 133.8 (ArC), 147.4 (ArC), 149.1 (ArC), 161.2 (ArC), 163.7 (ArC), 184.8 (C═S), 191.1 (ArC═S). APCI-MS(+) *m*/*z* 296.03 $[M + H]^+$. Anal. ($C_{13}H_{10}FNO_2S_2$). C, H, N, S, respectively: calcd 52.87, found 52.43; calcd 3.41, found 3.50; calcd 4.74, found 4.55; calcd 21.71, found 21.32.

3-Hydroxy-*N*-(4-methoxybenzyl)-4-oxo-4*H*-pyran-2-carboxamide (3a). 3a was prepared according to the same procedure outlined for **2a** starting from BPCA (1.0 g, 4.1 mmol), EDCI (786

mg, 4.1 mmol), HOBt (554 mg, 4.1 mmol), and 4-methoxybenzylamine (562 mg, 536 μL, 4.1 mmol) to yield an off-white solid of **3a** (600 mg, 2.2 mmol). Yield = 54%. ^{1}H NMR (400 MHz, $CDCl_3$, 25 °C): δ = 3.81 (s, 3H; OCH_3), 4.55 (d, J = 4.8 Hz, NHCH_2), 6.44 (d, J = 6 Hz, 1H; ArH), 6.89 (d, J = 8.8 Hz, 2H; ArH), 7.02 (brt, 1H; CONHCH$_2$), 7.26 (d, J = 9.6 Hz, 2H; ArH), 7.68 (d, J = 5.6 Hz, 1H; ArH). ^{13}C NMR (100 MHz, $CDCl_3$, 25 °C): δ = 43.1 (CH_2), 55.3 (OCH_3), 114.3 (ArC), 115.5 (ArC), 128.5 (ArC), 129.4 (ArC), 135.9 (ArC), 149.6 (ArC), 153.0 (ArC), 159.4 (ArC), 163.1 (C═O), 173.6 (ArC═O). ESI-MS(+) m/z 275.98 $[M + H]^+$. Anal. ($C_{14}H_{13}NO_5$) C, H, N.

3-Hydroxy-*N*-(4-methoxybenzyl)-4-thioxo-4*H*-pyran-2-carboxamide (3b). This compound was prepared from **3a** according to the procedure outlined for **1b**. **3a** (150 mg, 0.54 mmol) was treated with P_4S_{10} and HMDO for 1 h to yield an orange-red solid of **3b** (65 mg, 0.22 mmol). Yield = 41%. ^{1}H NMR (400 MHz, $CDCl_3$, 25 °C): δ = 3.77 (s, 3H; OCH_3), 4.56 (d, J = 5.2 Hz, NHCH_2), 6.85 (d, J = 8 Hz, 2H; ArH), 7.24 (d, J = 8.4 Hz, 2H; ArH), 7.36 (d, J = 4.8 Hz, 1H; ArH), 7.64 (d, J = 4.8 Hz, 1H; ArH), 7.80 (brt, 1H; CONHCH$_2$), 9.95 (brs, 1H; ArOH). ^{13}C NMR (100 MHz, $CDCl_3$, 25 °C): δ = 43.3 (CH_2), 55.2 (OCH_3), 114.1 (ArC), 125.9 (ArC), 128.8 (ArC), 129.1 (ArC), 132.0 (ArC), 146.9 (ArC), 151.6 (ArC), 159.1 (ArC), 160.8 (C═O), 190.6 (ArC═S). ESI-MS(−) m/z 290.09 $[M - H]^-$. Anal. ($C_{14}H_{13}NO_4S \cdot 0.35H_2O$). C, H, N, S, respectively: calcd 56.50, found 56.90; calcd 4.64, found 5.04; calcd 4.71, found 4.49; calcd 10.77, found 10.38.

3-Hydroxy-*N*-(4-methoxybenzyl)-4-thioxo-4*H*-pyran-2-carbothioamide (3c). 3c was obtained from **3a** from the same reaction as that of **3b** as a dark-brown solid (20 mg, 0.07 mmol). Yield = 7%. ^{1}H NMR (400 MHz, $CDCl_3$, 25 °C): δ = 3.82 (s, 3H; OCH_3), 4.87 (d, J = 5.6 Hz, NHCH_2), 6.91 (d, J = 8.8 Hz, 2H; ArH), 7.31 (d, J = 8.4 Hz, 2H; ArH), 7.40 (d, J = 4.8 Hz, 1H; ArH), 7.73 (d, J = 5.2 Hz, 1H; ArH), 9.38 (brt, 1H; CONHCH$_2$), 10.33 (brs, 1H; ArOH). ^{13}C NMR (100 MHz, $CDCl_3$, 25 °C): δ = 49.8 (CH_2), 55.2 (OCH_3), 114.2 (ArC), 125.3 (ArC), 127.1 (ArC), 129.6 (ArC), 133.6 (ArC), 147.0 (ArC), 149.4 (ArC), 159.4 (ArC), 184.2 (C═S), 191.2 (ArC═S). APCI-MS(−) m/z 306.06 $[M - H]^-$. Anal. ($C_{14}H_{13}NO_3S_2$) C, H, N, S.

***N*-Benzhydryl-3-hydroxy-4-oxo-4*H*-pyran-2-carboxamide (4a).** This compound was prepared according to the same procedure outlined for **3a** starting from BPCA (1.0 g, 4.1 mmol), EDCI (1.2 equiv, 939 mg, 4.9 mmol), HOBt (1.2 equiv, 662 mg, 4.9 mmol), and diphenylmethanamine (1.2 equiv, 898 mg, 844 μL, 4.9 mmol) to yield a tan solid of **4a** (732 mg, 2.3 mmol). Yield = 56%. ^{1}H NMR (400 MHz, $CDCl_3$, 25 °C): δ = 6.37 (d, J = 8 Hz, NHCH), 6.45 (d, J = 5.2 Hz, 1H; ArH), 7.05 (brd, J = 7.6 Hz, CONHCH$_2$), 7.28−7.43 (m, 10H; ArH), 7.72 (d, J = 6 Hz, 1H; ArH). ^{13}C NMR (100 MHz, DMSO-d_6, 25 °C): δ = 56.4 (CH_2), 114.4 (ArC), 127.3 (ArC), 128.5 (ArC), 137.7 (ArC), 141.2 (ArC), 147.9 (ArC), 155.2 (ArC), 160.8 (C═O), 173.5 (ArC═O). ESI-MS(+) m/z 321.85 $[M + H]^+$. Anal. ($C_{19}H_{15}NO_4 \cdot 0.25H_2O$). C, H, N: calcd 70.04, found 70.09; calcd 4.79, found 5.16; calcd 4.30, found 4.47.

***N*-Benzhydryl-3-hydroxy-4-thioxo-4*H*-pyran-2-carboxamide (4b).** This compound was prepared from **4a** according to the procedure outlined for **1b**. **4a** (600 mg, 1.9 mmol) was treated with P_4S_{10} and HMDO for 3 h to yield a light-brown solid of **4b** (90 mg, 0.27 mmol). Yield = 14%. ^{1}H NMR (400 MHz, $CDCl_3$, 25 °C): δ = 6.44 (d, J = 8 Hz, NHCH), 7.30−7.38 (m, 10H; ArH), 7.41 (d, J = 5.2 Hz, 1H; ArH), 7.70 (d, J = 4.8 Hz, 1H; ArH), 8.27 (brd, J = 7.2 Hz, CONHCH$_2$), 9.72 (brs, 1H; ArOH). ^{13}C NMR (100 MHz, DMSO-d_6, 25 °C): δ = 56.5 (ArC), 127.4 (ArC), 127.5 (ArC), 128.5 (ArC), 132.5 (ArC), 140.9 (ArC), 147.0 (ArC), 153.5 (ArC), 161.9 (C═O), 191.9 (ArC═S). APCI-MS(+) m/z 338.18 $[M + H]^+$. Anal. ($C_{19}H_{15}NO_3S \cdot 0.6H_2O$). C, H, N, S, respectively: calcd 65.54, found 65.60; calcd 4.69, found 5.05; calcd 4.02, found 4.02; calcd 9.21, found 10.33.

***N*-Benzhydryl-3-hydroxy-4-thioxo-4*H*-pyran-2-carbothioamide (4c). 4c** was obtained from **4a** from the same reaction as that of **4b** as a dark-brown solid (216 mg, 0.61 mmol). Yield = 32%. ^{1}H NMR (400 MHz, $CDCl_3$, 25 °C): δ = 6.93 (d, J = 7.2 Hz, NHCH), 7.30−7.40 (m, 10H; ArH), 7.42 (d, J = 5.2 Hz, 1H; ArH), 7.76 (d, J = 5.2 Hz, 1H; ArH), 9.92 (brd, CONHCH$_2$), 10.15 (brs, 1H; ArOH). ^{13}C NMR (100 MHz, DMSO-d_6, 25 °C): δ = 61.7 (CH_2), 125.5 (ArC), 127.6 (ArC), 127.7 (ArC), 128.6 (ArC), 139.2 (ArC), 139.7 (ArC), 147.7 (ArC), 184.4 (C═S), 191.1 (ArC═S). APCI-MS(+) m/z 353.85 $[M + H]^+$. Anal. ($C_{19}H_{15}NO_2S_2 \cdot 0.4H_2O$). C, H, N, S, respectively: calcd 63.27, found 63.47; calcd 4.42, found 4.86; calcd 3.88, found 3.90; calcd 17.78, found 18.16.

3-Hydroxy-*N*-(2-methoxybenzyl)-4-oxo-4*H*-pyran-2-carboxamide (5a). This compound was prepared according to the same procedure outlined for **3a** starting from BPCA (500 mg, 2.0 mmol), EDCI (1.2 equiv, 713 mg, 2.4 mmol), HOBt (1.2 equiv, 324 mg, 2.4 mmol), and 2-methoxybenzylamine (1.2 equiv, 329 mg, 310 μL, 2.4 mmol), to yield an off-white solid of **5a** (355 mg, 1.3 mmol). Yield = 65%. ^{1}H NMR (400 MHz, $CDCl_3$, 25 °C): δ = 3.86 (s, 3H; OCH_3), 4.57 (d, J = 3.6 Hz, NHCH_2), 6.39 (d, J = 5.2 Hz, 1H; ArH), 6.87 (q, J = 7.2 Hz, 2H; ArH), 7.25 (m, 2H; ArH), 7.57 (brt, 1H; CONHCH$_2$), 7.71 (d, J = 6 Hz, 1H; ArH). ^{13}C NMR (100 MHz, $CDCl_3$, 25 °C): δ = 39.6 (CH_2), 55.4 (OCH_3), 110.5 (ArC), 115.5 (ArC), 120.8 (ArC), 124.5 (ArC), 129.6 (ArC), 130.1 (ArC), 136.1 (ArC), 149.7 (ArC), 152.8 (ArC), 157.6 (ArC), 163.0 (C═O), 173.7 (ArC═O). APCI-MS(+) m/z 275.88 $[M + H]^+$. Anal. ($C_{14}H_{13}NO_5$) C, H, N.

3-Hydroxy-*N*-(2-methoxybenzyl)-4-thioxo-4*H*-pyran-2-carboxamide (5b). This compound was prepared from **5a** according to the procedure outlined for **1b**. **5a** (400 mg, 1.4 mmol) was treated with P_4S_{10} and HMDO for 2.5 h to yield a reddish brown solid of **5b** (290 mg, 1.0 mmol). Yield = 76%. ^{1}H NMR (300 MHz, $CDCl_3$, 25 °C): δ = 3.90 (s, 3H; OCH_3), 4.65 (d, J = 5.7 Hz, NHCH_2), 6.90 (q, J = 7.8 Hz, 2H; ArH), 7.28−7.35 (m, 2H; ArH), 7.40 (d, J = 4.8 Hz, 1H; ArH), 7.68 (d, J = 5.7 Hz, 1H; ArH), 8.08 (brt, 1H; CONHCH$_2$), 9.88 (brs, 1H; ArOH). ^{13}C NMR (75 MHz, $CDCl_3$, 25 °C): δ = 39.9 (CH_2), 55.4 (OCH_3), 110.4 (ArC), 120.7 (ArC), 125.0 (ArC), 125.8 (ArC), 129.4 (ArC), 129.9 (ArC), 133.4 (ArC), 147.0 (ArC), 152.1 (ArC), 157.6 (ArC), 161.4 (C═O), 191.7 (ArC═O). ESI-MS(+) m/z 292.00 $[M + H]^+$. HRMS calcd for $C_{14}H_{13}NO_4S$: 291.0560. Found: 291.0563.

3-Hydroxy-*N*-(2-methoxybenzyl)-4-thioxo-4*H*-pyran-2-carbothioamide (5c). 5c was obtained from **5a** from the same reaction as that of **5b** as a dark-brown solid (90 mg, 0.29 mmol). Yield = 21%. ^{1}H NMR (400 MHz, $CDCl_3$, 25 °C): δ = 3.90 (s, 3H; OCH_3), 4.99 (d, J = 5.2 Hz, NHCH_2), 6.93 (q, J = 7.2 Hz, 2H; ArH), 7.33 (q, J = 8 Hz, 2H; ArH), 7.40 (d, J = 5.2 Hz, 1H; ArH), 7.73 (d, J = 5.2 Hz, 1H; ArH), 9.70 (brt, 1H; CONHCH$_2$), 10.43 (brs, 1H; ArOH). ^{13}C NMR (100 MHz, $CDCl_3$, 25 °C): δ = 45.4 (CH_2), 55.1 (OCH_3), 110.3 (ArC), 120.4 (ArC), 122.9 (ArC), 125.7 (ArC), 129.5 (ArC), 130.2 (ArC), 133.6 (ArC), 146.4 (ArC), 150.1 (ArC), 157.4 (ArC), 183.6 (C═S), 191.8 (ArC═S). APCI-MS(+) m/z 307.91 $[M + H]^+$. Anal. ($C_{14}H_{13}NO_3S_2 \cdot 0.5H_2O$). C, H, N, S, respectively: calcd 53.15, found 52.90; calcd 4.46, found 4.49; calcd 4.43, found 4.12; calcd 20.27, found 20.44.

3-Hydroxy-*N*-(3-methoxybenzyl)-4-oxo-4*H*-pyran-2-carboxamide (6a). This compound was prepared according to the same procedure outlined for **3a** starting from BPCA (500 mg, 2.0 mmol), EDCI (1.2 equiv, 713 mg, 2.4 mmol), HOBt (1.2 equiv, 324 mg, 2.4 mmol), and 3-methoxybenzylamine (1.2 equiv, 329 mg, 310 μL, 2.4 mmol) to yield a tan solid of **6a** (330 mg, 1.2 mmol). Yield = 60%. ^{1}H NMR (400 MHz, $CDCl_3$, 25 °C): δ = 3.79 (s, 3H; OCH_3), 4.57 (d, J = 4.8 Hz, NHCH_2), 6.52 (d, J = 6.0 Hz, 1H; ArH), 6.82−6.92 (m, 3H; ArH), 7.24 (t, J = 7.8 Hz, 1H; ArH), 7.60 (brt, 1H; CONHCH$_2$), 7.81 (d, J = 5.2 Hz, 1H; ArH). ^{13}C NMR (100 MHz, $CDCl_3$, 25 °C): δ = 43.5 (CH_2), 55.3 (OCH_3), 113.2 (ArC), 113.4 (ArC), 113.7 (ArC), 120.1 (ArC), 130.0 (ArC), 136.0 (ArC), 138.1 (ArC), 149.6 (ArC), 153.1 (ArC), 159.9 (ArC), 163.1 (C═O), 173.6 (ArC═O). APCI-MS(+) m/z 275.96 $[M + H]^+$. Anal. ($C_{14}H_{13}NO_5$) C, H, N.

3-Hydroxy-*N*-(3-methoxybenzyl)-4-thioxo-4*H*-pyran-2-carboxamide (6b). This compound was prepared from **6a** according to the procedure outlined for **1b**. **6a** (40 mg, 0.15 mmol) was treated with P_4S_{10} and HMDO for 40 min to yield a brown solid of **6b** (40 mg, 0.14 mmol). Yield = 95%. ^{1}H NMR (300 MHz, $CDCl_3$, 25 °C): δ = 3.81 (s, 3H; OCH_3), 4.64 (d, J = 6.0 Hz, NHCH_2),

6.83−6.89 (m, 2H; ArH), 6.92 (d, J = 7.8 Hz, 1H; ArH), 7.28 (d, J = 7.8 Hz, 1H; ArH), 7.41 (d, J = 5.4 Hz, 1H; ArH), 7.70 (d, J = 4.8 Hz, 1H; ArH), 7.86 (brt, 1H; CON*H*CH_2), 9.74 (brs, 1H; ArOH). ^{13}C NMR (75 MHz, DMSO-d_6, 25 °C): δ = 42.4 (CH_2), 55.0 (OCH_3), 112.5 (ArC), 113.2 (ArC), 119.5 (ArC), 127.8 (ArC), 129.5 (ArC), 131.7 (ArC), 139.6 (ArC), 154.1 (ArC), 159.3 (ArC), 161.9 (ArC), 163.4 (C═O), 192.4 (ArC═S). ESI-MS(+) *m*/*z* 292.05 $[M + H]^+$. HRMS calcd for $C_{14}H_{13}NO_3S$: 291.0560. Found: 291.0556.

3-Hydroxy-*N*-(3-methoxybenzyl)-4-thioxo-4*H*-pyran-2-carbothioamide (6c). This compound was prepared from **6a** according to the procedure outlined for **1c**. **6a** (450 mg, 1.6 mmol) was treated for 2 h to yield a dark-greenish-brown solid of **6c** (126 mg, 0.43 mmol). Yield = 27%. ^{1}H NMR (400 MHz, $CDCl_3$, 25 °C): δ = 3.83 (s, 3H; O*C*H_3), 4.93 (d, J = 5.2 Hz, NH*C*H_2), 6.89−6.92 (m, 2H; ArH), 6.96 (d, J = 8.0 Hz, 1H; ArH), 7.30 (t, J = 8.0 Hz, 1H; ArH), 7.42 (d, J = 5.2 Hz, 1H; ArH), 7.76 (d, J = 5.2 Hz, 1H; ArH), 9.47 (brt, 1H; CON*H*CH_2), 10.26 (brs, 1H; ArOH). ^{13}C NMR (75 MHz, $CDCl_3$, 25 °C): δ = 50.4 (CH_2), 55.3 (OCH_3), 113.6 (ArC), 113.9 (ArC), 120.4 (ArC), 125.2 (ArC), 129.2 (ArC), 130.2 (ArC), 133.9 (ArC), 136.8 (ArC), 147.5 (ArC), 160.0 (ArC), 185.3 (C═S), 197.0 (ArC═S). APCI-MS(+) *m*/*z* 307.96 $[M + H]^+$. Anal. ($C_{14}H_{13}NO_3S_2 \cdot 0.55H_2O$). C, H, N, S, respectively: calcd 52.99, found 52.83; calcd 4.48, found 4.57; calcd 4.41, found 4.40; calcd 20.21, found 21.52.

***N*-Benzyl-3-hydroxy-4-oxo-4*H*-pyran-2-carboxamide (7a).** This compound was prepared according to the same procedure outlined for **3a** starting from BPCA (575 mg, 2.3 mmol), EDCI (1.0 equiv, 441 mg, 2.3 mmol), HOBt (1.0 equiv, 311 mg, 2.3 mmol), and benzylamine (1.0 equiv, 246 mg, 251 μL, 2.3 mmol) to yield a tan solid of **7a** (294 mg, 1.2 mmol). Yield = 52%. ^{1}H NMR (400 MHz, $CDCl_3$, 25 °C): δ = 4.63 (d, J = 6 Hz, NH*C*H_2), 6.46 (d, J = 5.2 Hz, 1H; ArH), 7.04 (brt, 1H; CON*H*CH_2), 7.34−7.41 (m, 5H; ArH), 7.69 (d, J = 6 Hz, 1H; ArH). ^{13}C NMR (100 MHz, $CDCl_3$, 25 °C): δ = 43.6 (CH_2), 115.5 (ArC), 128.0 (ArC), 128.1 (ArC), 129.0 (ArC), 135.9 (ArC), 136.5 (ArC), 149.6 (ArC), 153.0 (ArC), 163.1 (C═O), 173.5 (ArC═O). APCI-MS(+) *m*/*z* 246.00 $[M + H]^+$. Anal. ($C_{13}H_{11}NO_4$) C, H, N.

***N*-Benzyl-3-hydroxy-4-thioxo-4*H*-pyran-2-carboxamide (7b).** This compound was prepared from **7a** according to the procedure outlined for **1b**. **7a** (250 mg, 1.0 mmol) was treated for 1.5 h to yield a mustard-brown solid of **7b** (85 mg, 0.32 mmol). Yield = 32%. ^{1}H NMR (300 MHz, $CDCl_3$, 25 °C): δ = 4.51 (d, J = 6 Hz, NH*C*H_2), 7.15−7.20 (m, 1H; ArH), 7.23 (s, 3H; ArH), 7.24 (s, 1H; ArH), 7.27 (d, J = 4.4 Hz, 1H; ArH), 7.58 (d, 7.04, J = 4.4 Hz, 1H; ArH), 8.29 (brt, 1H; CON*H*CH_2), 9.80 (brs, 1H; ArOH). ^{13}C NMR (75 MHz, DMSO-d_6, 25 °C): δ = 43.3 (CH_2), 126.3 (ArC), 127.4 (ArC), 127.5 (ArC), 128.5 (ArC), 131.5 (ArC), 136.7 (ArC), 146.4 (ArC), 152.2 (ArC), 161.7 (C═S), 191.1 (ArC═S). APCI-MS(+) *m*/*z* 262.05 $[M + H]^+$. HRMS calcd for $C_{13}H_{11}NO_3S$: 261.0454. Found: 291.0455.

***N*-Benzyl-3-hydroxy-4-thioxo-4*H*-pyran-2-carbothioamide (7c).** This compound was prepared from **7a** according to the procedure outlined for **1c**. **7a** (180 mg, 0.73 mmol) was treated with P_4S_{10} and HMDO for 2.5 h to yield a dark-red solid of **7c** (24 mg, 0.09 mmol). Yield = 12%. ^{1}H NMR (400 MHz, $CDCl_3$, 25 °C): δ = 4.961 (d, J = 5.2 Hz, NH*C*H_2), 7.347−7.393 (m, 5H; ArH), 7.409 (d, J = 5.2 Hz, 1H; ArH), 7.744 (d, J = 5.2 Hz, 1H; ArH), 9.473 (brt, 1H; CON*H*CH_2), 10.305 (brs, 1H; ArOH). ^{13}C NMR (100 MHz, $CDCl_3$, 25 °C): δ = 50.021 (CH_2), 125.403 (ArC), 128.042 (ArC), 128.149 (ArC), 128.855 (ArC), 133.563 (ArC), 135.079 (ArC), 146.847 (ArC), 149.639 (ArC), 184.477 (C═S), 191.316 (ArC═S). APCI-MS(+) *m*/*z* 278.08 $[M + H]^+$. Anal. ($C_{13}H_{11}NO_2S_2 \cdot 0.5H_2O$). C, H, N, S, respectively: calcd 54.52, found 54.69; calcd 4.22, found 4.62; calcd 5.71, found 4.89; calcd 22.39, found 21.89.

***N*-Ethyl-3-hydroxy-4-oxo-4*H*-pyran-2-carboxamide (8a).** This compound was prepared according to the same procedure outlined for **3a** starting from BPCA (500 mg, 2.0 mmol), EDCI (1.2 equiv, 713 mg, 2.4 mmol), HOBt (1.2 equiv, 324 mg, 2.4 mmol), and 2 M ethylamine in THF (1.2 equiv, 1.2 mL, 2.4 mmol) to yield an off-white solid of **8a** (210 mg, 1.2 mmol). Yield = 64%. ^{1}H NMR (400 MHz, $CDCl_3$, 25 °C): δ = 1.26 (t, J =7.4 Hz, 2H; CH_2CH_3), 3.47 (p, J = 7.2 Hz, 2H; NH*C*H_2CH_3), 6.46 (d, J = 5.2 Hz, 1H; ArH), 6.75 (brt, 1H; CON*H*CH_2), 7.71 (d, J = 5.6 Hz, 1H; ArH). ^{13}C NMR (100 MHz, $CDCl_3$, 25 °C): δ = 14.6 (CH_2CH_3), 34.6 (CH_2CH_3), 115.5 (ArC), 136.0 (ArC), 149.5 (ArC), 152.9 (ArC), 163.2 (C═O), 173.7 (ArC═O). ESI-MS(+) *m*/*z* 184.09 $[M + H]^+$. HRMS calcd for $C_8H_9NO_4$: 183.0526. Found: 183.0525.

***N*-Ethyl-3-hydroxy-4-thioxo-4*H*-pyran-2-carboxamide (8b).** This compound was prepared from **8a** according to the procedure outlined for **1b**. **8a** (107 mg, 0.6 mmol) was treated with P_4S_{10} and HMDO for 25 min to yield a reddish-brown solid of **8b** (30 mg, 0.15 mmol). Yield = 25%. ^{1}H NMR (300 MHz, $CDCl_3$, 25 °C): δ = 1.26 (t, J = 7.4 Hz, 2H; CH_2CH_3), 3.50 (p, J = 7.0 Hz, 2H; CH_2CH_3), 7.42 (d, J = 5.2 Hz, 1H; ArH), 7.71 (brt, 1H; CON*H*CH_2), 7.70 (d, J = 5.2 Hz, 1H; ArH), 9.86 (brs, 1H; ArOH). ESI-MS(+) *m*/*z* 222.02 $[M + Na]^+$. HRMS calcd for $C_8H_9NO_3SNa$: 222.0195. Found: 222.0193.

***N*-Ethyl-3-hydroxy-4-thioxo-4*H*-pyran-2-carbothioamide (8c).** This compound was prepared from **8a** according to the procedure outlined for **1c**. **8a** (165 mg, 0.90 mmol) was treated for 2.5 h to yield a dark-brown solid of **8c** (77 mg, 0.36 mmol). Yield = 40%. ^{1}H NMR (400 MHz, $CDCl_3$, 25 °C): δ = 1.38 (t, J = 7.4 Hz, 2H; CH_2CH_3), 3.81−3.88 (m, 2H; CH_2CH_3), 7.41 (d, J = 5.2 Hz, 1H; ArH), 7.74 (d, J = 4.8 Hz, 1H; ArH), 9.21 (brt, 1H; CON*H*CH_2), 10.44 (brs, 1H; ArOH). ^{13}C NMR (100 MHz, $CDCl_3$, 25 °C): δ = 12.9 (CH_2CH_3), 41.1 (CH_2CH_3), 125.3 (ArC), 133.7 (ArC), 147.1 (ArC), 149.3 (ArC), 184.6 (C═S), 191.4 (ArC═S). APCI-MS(+) *m*/*z* 216.01 $[M + H]^+$. Anal. ($C_8H_9NO_2S_2$). C, H, N, S, respectively: calcd 44.63, found 44.89; calcd 4.21, found 4.70; calcd 6.51, found 6.51; calcd 29.79, found 30.34.

***N*-(Biphenyl-4-ylmethyl)-1-hydroxy-6-oxo-1,6-dihydropyridine-2-carboxamide (9a).** This compound was prepared as previously reported.[46]

***N*-(4-Fluorobenzyl)-1-hydroxy-6-oxo-1,6-dihydropyridine-2-carboxamide (10a).** To a solution of 1-(benzyloxy)-6-oxo-1,6-dihydropyridine-2-carboxylic acid (BDCA)[46] (200 mg, 0.82 mmol) in dichloromethane was added EDCI (1.0 equiv, 157 mg, 0.82 mmol), HOBt (1.0 equiv, 111 mg, 0.82 mmol), and 4-fluorobenzylamine (1.0 equiv, 93 μL, 0.82 mmol). The mixture was stirred overnight at room temperature under N_2 and then poured into a separatory funnel and extracted with water and dichloromethane. The organic layers were combined, dried over anhydrous magnesium sulfate, filtered, and concentrated to give the benzyl-protected intermediate. The intermediate was dissolved in 10 mL of a 1:1 solution of concentrated HCl and glacial acetic acid. The reaction mixture was stirred for 5 d and then concentrated in vacuo, coevaporated with MeOH, and dried to yield an off-white solid (55 mg, 0.21 mmol). Yield = 26%. ^{1}H NMR (400 MHz, $CDCl_3$, 25 °C): δ = 4.51 (d, J = 5.6 Hz, 2H; NH*C*H_2), 6.88 (q, J = 9.0 Hz, 2H; ArH), 7.23 (m, 4H; ArH), 7.41 (t, J = 8.0 Hz, 1H; ArH), 9.66 (br t, 1H; CON*H*CH_2). APCI-MS(+) *m*/*z* 263.01 $[M + H]^+$.

2-Bromopyridine-6-carboxylic Acid 1-Oxide (BCAO). The synthesis is based on a modified literature procedure.[48] To 6-bromopicolinic acid (6-BPA) (2.0 g, 9.9 mmol) was added a solution of 26 mL of trifluoroacetic acid and 4 mL of 30% hydrogen peroxide. The reaction mixture was heated to reflux at 80 °C for 7 h under N_2. The solution was concentrated in vacuo and the concentrate was added to 200 mL of water, which resulted in the immediate formation of a precipitate. The precipitate was vacuum-filtered and dried to afford an off-white solid (2.03 g, 9.3 mmol). Yield = 94%. ^{1}H NMR (400 MHz, DMSO-d_6, 25 °C): δ 7.69 (t, J = 8.0 Hz, 1H; ArH), 8.24 (dd, J = 6.0, 10.4 Hz, 1H; ArH), 8.30 (dd, J = 5.6, 10.4 Hz, 1H; ArH). ESI-MS(−): *m*/*z* 215.86 $[M - H]^-$.

1-Hydroxy-6-thioxo-1,6-dihydropyridine-2-carboxylic Acid (HTDCA). The synthesis is based on a modified literature procedure.[47] BCAO (3.0 g, 14.0 mmol) was dissolved in a 50 mL solution of $Na_2S \cdot 9H_2O$ (3.3 g, 14 mmol) at 70 °C. To this yellow solution was added 14 mmol of NaHS in 50 mL of water, and the pH was adjusted to 10. The resulting reaction mixture was heated to reflux

at 95 °C for 6 h under N_2 and acidified while still hot with concentrated HCl to pH 2. The solution was concentrated in vacuo and the resulting precipitate was vacuum-filtered to yield a crude yellow crystalline solid. The crude acid was partially dissolved in dichloromethane and extracted 2× with 5 M NaOH. The aqueous phase was acidified to pH 1 with concentrated HCl and was further extracted 3× with dichloromethane. The organic phase was dried over anhydrous magnesium sulfate that was then vacuum-filtered off. The filtrate was concentrated to yield a pure bright-yellow solid (2.1 g, 12.3 mmol). Yield = 88%. ^{1}H NMR (400 MHz, $CDCl_3$, 25 °C): δ 7.48 (t, J = 8.0 Hz, 1H; ArH), 7.67 (dd, J = 5.6, 10.4 Hz, 1H; ArH), 8.18 (dd, J = 6.0, 9.6 Hz, 1H; ArH). APCI-MS(+): m/z 172.12 $[M + H]^+$. HR-EI-MS calcd for $C_6H_5NO_3S$ 170.9984. Expected 170.9985. Anal. ($C_6H_5NO_3S$) C, H, N.

***N*-(Biphenyl-4-ylmethyl)-1-hydroxy-6-thioxo-1,6-dihydropyridine-2-carboxamide (9b).** To a solution of HTDCA (105 mg, 0.6 mmol) in dichloromethane was added NHS (1.0 equiv, 70 mg, 0.6 mmol), EDCI (1.0 equiv, 117 mg, 0.6 mmol), and 4-phenylbenzylamine (1.0 equiv, 112 mg, 0.6 mmol). The mixture was stirred overnight at room temperature under N_2 and then poured into a separatory funnel and extracted with saturated $NaHCO_3$ and dichloromethane. The organic layers were combined, dried over anhydrous magnesium sulfate, filtered, and concentrated to a yellow residue. The crude residue was purified via silica column chromatography (1% MeOH/$CHCl_3$). Maltol (3-hydroxy-2-methyl-4*H*-pyran-4-one) was first run through the column to remove any metal impurities in the silica. The compound **9b** was isolated as a yellow solid after removal of solvent (94 mg, 0.3 mmol). Yield = 46%. ^{1}H NMR (400 MHz, $CDCl_3$, 25 °C): δ 4.73 (d, J = 6.0 Hz, 2H; NHC*H*$_2$,), 7.33 (t, J = 6.4 Hz, 1H; ArH), 7.42−7.59 (m, 9H; ArH), 7.67 (dd, J = 6.4, 10.0 Hz, 1H; ArH), 8.32 (dd, J = 6.0, 10.0 Hz, 1H; ArH), 11.17 (t, J = 5.8 Hz, 1H; N*H*CH$_2$). APCI-MS(−): m/z 335.04 $[M - H]^-$. Anal. ($C_{19}H_{16}N_2O_2$). C, H, N, S, respectively: calcd 67.84, found 67.36; calcd 4.79, found 5.06; calcd 8.33, found 8.13; calcd 9.53, found 9.32.

***N*-(4-Fluorobenzyl)-1-hydroxy-6-thioxo-1,6-dihydropyridine-2-carboxamide (10b).** The synthesis of **10b** was performed as described for **9b**, starting from HTDCA (50 mg, 0.3 mmol), EDCI (1.0 equiv, 56 mg, 0.3 mmol), HOBt (1.0 equiv, 39 mg, 0.3 mmol), and 4-fluorobenzylamine (1.0 equiv, 36 mg, 33 μL, 0.3 mmol). Yield = 95%. ^{1}H NMR (400 MHz, $CDCl_3$, 25 °C): δ 4.65 (d, J = 6.0 Hz, 2H; NHC*H*$_2$,), 7.01 (t, J = 8.8 Hz, 2H; ArH), 7.34 (qd, J = 3.2, 4.8 Hz, 2H; ArH), 7.43 (t, J = 8.4 Hz, 1H; ArH), 7.66 (dd, J = 6.4, 10.4 Hz, 1H; ArH), 8.30 (dd, J = 6.8, 9.6 Hz, 1H; ArH), 11.13 (t, J = 5.6 Hz, 1H; N*H*CH$_2$). APCI-MS(−): m/z 276.96 $[M - H]^-$.

Single-Crystal X-ray Diffraction. A single crystal of **5c** suitable for X-ray diffraction structural determination was mounted on a nylon loop with Paratone oil and placed under a nitrogen cold stream (100 K). Data were collected on a Bruker P4 diffractometer using Mo Kα radiation (λ = 0.710 73 Å) controlled using the APEX 2.0 software package. A semiempirical method utilizing equivalents was employed to correct for absorption.[62] The data collection was solved and refined using SHELXTL suite. All hydrogen atoms were fixed at calculated positions with isotropic thermal parameters, while all non-hydrogen atoms were refined anisotropically.

Inhibition Assays. The compounds were dissolved in dimethyl sulfoxide (DMSO) at a concentration of 50 mM. Serial dilutions of the inhibitor were made from this stock and were diluted 500× in LF buffer (20 mM HEPES, 1 mM $CaCl_2$, 0.1 mg/mL BSA, 0.01% Tween-20, pH 7). The assay was carried out in 96-well plates. Each well contained a total volume of 100 μL = 25 μL buffer, 10 nM (30 μL) recombinant LF (List Biological Laboratories), 20 μL LFi, and the reaction was initiated by the addition of 3 μM (25 μL) fluorogenic LF substrate (Cou)-*N*-Nle-Lys-Lys-Lys-Lys-Val-Leu-Pro-Ile-Gln-Leu-Asn-Ala-Ala-Thr-Asp-Lys-(QSY-35)-Gly-Gly-NH_2 (Calbiochem) after a 35 min incubation period at 25 °C. Kinetic measurements were recorded every minute for 15 min with excitation and emission wavelengths at 380 and 450 nm, respectively.

Construction of an Inhibitor/Anthrax LF Complex Model. Our starting structure was the complex from Lewis et al.,[40] in which **11b** is in the anthrax lethal factor (LF) active site. The 6-methyl group of **11b** was replaced with a hydrogen atom to construct inhibitor **1b**. The inhibitor **1c** was obtained by replacing the carbonyl oxygen atom of **1b** with a sulfur atom. The atomic charges for both **1b** and **1c** were derived by fitting to HF/6-31G* electrostatic potentials (ESP) using the RESP module. Other force parameters for the two inhibitors were adapted from the standard force field by following the general parametrization procedures outlined in AMBER manual.[63,64] After the added atoms in the gas phase were relaxed, each structure was immersed in a cubic TIP3P water box and neutralized by addition of Na^+ counterions using the AMBER Leap module. This led to the [**1b**·LF] (or [**1c**·LF]) simulation system of 55 268 atoms. MD simulations were conducted in the NPT ensemble at 300 K and 1 atm. The SHAKE algorithm[65] was used to constrain all bond lengths involving hydrogens. A 10.0 Å cutoff was used for nonbonded interactions, and the neighbor pair list was updated every 10 steps. The long-range electrostatic interactions were treated with the particle mesh Ewald method.[66] The two prepared systems were first equilibrated with a series of minimizations interspersed by short MD simulations, and then two snapshots from two models were selected for the following QM/MM investigations. These selected structures were first minimized using the MM method and then optimized with the B3LYP(6-31G*) QM/MM calculations using an iterative minimization approach.[67]

QM/MM Minimization Calculations. The pseudobond ab initio QM/MM approach[68,69] has achieved great success in accurate modeling of the chemistry at an enzyme active site while properly including the effects of the enzymatic environment. It has been applied to various enzyme reactions, including enolase,[70] acetylcholinesterase,[71] 4-oxalocrotonate tautomerase,[72] kinase,[73] and methyl transferase.[74] The QM/MM approach divides the whole enzyme−substrate system into a QM and a MM subsystem. The active site of the enzyme was described by a QM Hamiltonian, and the influence of the remainder of the protein and the solvent was included via a coupled MM potential. The code combining the modified Gaussian 98[74] and Tinker 3.6[75] was utilized for all the calculations. An efficient iterative optimization procedure[67] was repeatedly applied to minimize the enzyme−substrate system into a local minimum. For each minimization cycle, the large MM subsystem was relaxed with the truncated Newton method in Cartesian coordinates while the small QM subsystem was treated using the quasi-Newton minimizer at the B3LYP/6-31G* level in redundant internal coordinates. For the QM/MM calculations on the [**1b**·LF] and [**1c**·LF] models, the QM subsystem consists of the side chain of His422, His426, Glu471, zinc(II), and **1b** (or **1c**), resulting in a total of 70 QM atoms. Geometry optimizations for both the QM subgroups were at the B3LYP(6-31G*) level, with the boundary between the QM and MM subsystems treated using the pseudobond approach.[69] The scheme used in our QM/MM calculations corresponds to a good compromise between accuracy and computational cost. While being economical for the large system size, B3LYP is quite reliable for geometry optimizations including those of Zn(II) complexes, which is the primary issue in this work. More accurate schemes are available where computational requirements may be more demanding.[76] All other atoms are described by the classical MM force fields. Similarly, we constructed the [**2b**·LF] and [**2c**·LF], [**3b**·LF] and [**3c**·LF], and [**7b**·LF] and [**7c**·LF] QM/MM models.

Acknowledgment. The authors thank Kristine K. Tanabe for solving the crystal structure of **5c** and Dr. Yongxuan Su (University of California, San Diego) for obtaining the mass spectrometry data. This work has been supported by a grant from the National Institutes of Health (S.M.C., Grant R03 AI070651-01) and in part by grants from NSF, NIH, the Center for Theoretical Biological Physics, the National Biomedical Computation Resource, NSF Supercomputing Centers, and Accelrys, Inc. (J.A.M).

Supporting Information Available: Crystallographic information for compound **5c** in CIF format, results from combustion analysis, table of crystallographic data collection and structural parameters for **5c**, and structural diagram of **5c**. This material is available free of charge via the Internet at http://pubs.acs.org.

References

(1) Pile, J. C.; Malone, J. D.; Eitzen, E. M.; Friedlander, A. M. Anthrax as a potential biological warfare agent. *Arch. Intern. Med.* **1998**, *158*, 429–434.

(2) Collier, R. J.; Young, J. A. T. Anthrax toxin. *Annu. Rev. Cell Dev. Biol.* **2003**, *19*, 45–70.

(3) Smith, H.; Keppie, J. Observations on experimental anthrax: demonstration of a specific lethal factor produced in vivo by *Bacillus anthracis*. *Nature* **1954**, *173*, 869–870.

(4) Tournier, J. N.; Quesnel-Hellmann, A.; Cleret, A.; Vidal, D. R. Contribution of toxins to the pathogenesis of inhalational anthrax. *Cell. Microbiol.* **2007**, *9*, 555–565.

(5) Bradley, K. A.; Mogridge, J.; Mourez, M.; Collier, R. J.; Young, J. A. T. Identification of the cellular receptor for anthrax toxin. *Nature* **2001**, *414*, 225–229.

(6) Miller, C. J.; Elliot, J. L.; Collier, R. J. Anthrax protective antigen: prepore-to-pore conversion. *Biochemistry* **1999**, *38*, 10432–10441.

(7) Scobie, H. M.; Rainey, J. A.; Bradley, K. A.; Young, J. A. T. Human capillary morphogenesis protein 2 functions as an anthrax toxin receptor. *Proc. Natl. Acad. Sci. U.S.A.* **2003**, *100*, 5170–5174.

(8) Young, J. A.; Collier, R. J. Anthrax toxin: receptor binding, internalization, pore formation, and translocation. *Annu. Rev. Biochem.* **2007**, *76*, 243–265.

(9) Krantz, B. A.; Finkelstein, A.; Collier, R. J. Protein translocation through the anthrax toxin transmembrane pore is driven by a proton gradient. *J. Mol. Biol.* **2006**, *355*, 968–979.

(10) Leppla, S. H. Anthrax toxin edema factor: a bacterial adenylate cyclase that increases cyclic AMP concentrations in eukaryotic cells. *Proc. Natl. Acad. Sci. U.S.A.* **1982**, *79*, 3162–3166.

(11) Paccani, S. R.; Tonello, F.; Patrussi, L.; Capitani, N.; Simonato, M.; Montecucco, C.; Baldari, C. T. Anthrax toxins inhibit immune cell chemotaxis by perturbing chemokine receptor signalling. *Cell. Microbiol.* **2007**, *9*, 924–929.

(12) Scobie, H. M.; Marlett, J. M.; Rainey, G. J. A.; Lacy, D. B.; Collier, R. J.; Young, J. A. T. Anthrax toxin receptor 2 determinants that dictate the pH threshold of toxin pore formation. *PLoS One* **2007**, *2*, e329.

(13) Sun, J.; Lang, A. E.; Aktories, K.; Collier, R. J. Phenylalanine-427 of anthrax protective antigen functions in both pore formation and protein translocation. *Proc. Natl. Acad. Sci. U.S.A.* **2008**, *105*, 4346–4351.

(14) Wimalasena, D. S.; Cramer, J. C.; Janowiak, B. E.; Jurius, S. J.; Melnyk, R. A.; Anderson, D. E.; Kirk, K. L.; Collier, R. J.; Bann, J. G. Effect of 2-fluorohistidine labeling of the anthrax protective antigen on stability, pore formation, and translocation. *Biochemistry* **2007**, *46*, 14928–14936.

(15) Agrawal, A.; Pulendran, B. Anthrax lethal toxin: a weapon of multisystem destruction. *Cell. Mol. Life Sci.* **2004**, *61*, 2859–2865.

(16) Park, J. M.; Greten, F. R.; Li, Z. W.; Karin, M. Macrophage apoptosis by anthrax lethal factor through p38 MAP kinase inhibition. *Science* **2002**, *297*, 2048–2051.

(17) Chopra, A. P.; Boone, S. A.; Liang, X.; Duesbery, N. S. Anthrax lethal factor proteolysis and inactivation of MAPK kinase. *J. Biol. Chem.* **2003**, *278*, 9402–9406.

(18) Puhar, A.; Montecucco, C. Where and how do anthrax toxins exit endosomes to intoxicate host cells? *Trends Microbiol.* **2007**, *15*, 477–482.

(19) Tonello, F.; Ascenzi, P.; Montecucco, C. The metalloproteolytic activity of the anthrax lethal factor is substrate-inhibited. *J. Biol. Chem.* **2003**, *278*, 40075–40078.

(20) Ascenzi, P.; Visca, P.; Ippolito, G.; Spallarossa, A.; Bolognesi, M.; Montecucco, C. Anthrax toxin: a tripartite lethal combination. *FEBS Lett.* **2002**, *531*, 384–388.

(21) Hanna, P. C.; Acosta, D.; Collier, R. J. On the role of macrophages in anthrax. *Proc. Natl. Acad. Sci. U.S.A.* **1993**, *90*, 10198–10201.

(22) Pezard, C.; Berche, P.; Mock, M. Contribution of individual toxin components to virulence of *Bacillus anthracis*. *Infect. Immun.* **1991**, *59*, 3472–3477.

(23) Forino, M.; Johnson, S. L.; Wong, T. Y.; Rozanov, D. V.; Savinov, A. Y.; Li, W.; Fattorusso, R.; Becattini, B.; Orry, A. J.; Jung, D.; Abagyan, R. A.; Smith, J. W.; Alibek, K.; Liddington, R. C.; Strongin, A. Y.; Pellecchia, M. Efficient synthetic inhibitors of anthrax lethal factor. *Proc. Natl. Acad. Sci. U.S.A.* **2005**, *2005*, 9499–9504.

(24) Gaddis, B. D.; Avramova, L. V.; Chmielewski, J. Inhibitors of anthrax lethal factor. *Bioorg. Med. Chem. Lett.* **2007**, *17*, 4575–4578.

(25) Jiao, G. S.; Simo, O.; Nagata, M.; O'Malley, S.; Hemscheidt, T.; Cregar, L.; Millis, S. Z.; Goldman, M. E.; Tang, C. Selectively guanidinylated derivatives of neamine. Synthesis and inhibition of anthrax lethal factor protease. *Bioorg. Med. Chem. Lett.* **2006**, *16*, 5183–5189.

(26) Johnson, S. L.; Chen, L. H.; Pellecchia, M. A high-througput screening approach to anthrax lethal factor inhibition. *Bioorg. Chem.* **2007**, *35*, 306–312.

(27) Johnson, S. L.; Jung, D.; Forino, M.; Chen, Y.; Satterhwait, A.; Rozanov, D. V.; Strongin, A. Y.; Pellecchia, M. Anthrax lethal factor protease inhibitors: synthesis, SAR, and structure-based 3D QSAR studies. *J. Med. Chem.* **2006**, *49*, 27–30.

(28) Johnson, S. L.; Pellecchia, M. Structure- and fragment-based approaches to protease inhibition. *Curr. Top. Med. Chem.* **2006**, *6*, 317–329.

(29) Numa, M. M. D.; Lee, L. V.; Hsu, C. C.; Bower, K. E.; Wong, C. H. Identification of novel anthrax lethal factor inhibitors generated by combinatorial Pictet−Spengler reaction followed by screening in situ. *ChemBioChem* **2005**, *2005*, 1002–1006.

(30) Panchal, R. G.; Hermone, A. R.; Nguyen, T. L.; Wong, T. Y.; Schwarzenbacher, R.; Schmidt, J.; Lane, D.; McGrath, C.; Turk, B. E.; Burnett, J.; Aman, M. J.; Little, S.; Sausville, E. A.; Zaharevitz, D. W.; Cantley, L. C.; Liddington, R. C.; Gussio, R.; Bavari, S. Identification of small molecule inhibitors of anthrax lethal factor. *Nat. Struct. Mol. Biol.* **2004**, *11*, 67–72.

(31) Schepetkin, I. A.; Khlebnikov, A. I.; Kirpotina, L. N.; Quinn, M. T. Novel small-molecule inhibitors of anthrax lethal factor identified by high-throughput screening. *J. Med. Chem.* **2006**, *49*, 5232–5244.

(32) Shoop, W. L.; Xiong, Y.; Wiltsie, J.; Woods, A.; Guo, J.; Pivnichny, J. V.; Felcetto, T.; Michael, B. F.; Bansal, A. C., R. T.; Cunningham, B. R.; Friedlander, A. M.; Douglas, C. M.; Patel, S. B.; Wisniewski, D.; Scapin, G.; Salowe, S. P.; Zaller, D. M.; Chapman, K. T.; Scolnick, E. M.; Schmatz, D. M.; Bartizal, K.; MacCoss, M. Anthrax lethal factor inhibition. *Proc. Natl. Acad. Sci. U.S.A.* **2005**, *102*, 7958–7963.

(33) Turk, B. E.; Wong, T. Y.; Schwarzenbacher, R.; Jarrell, E. T.; Leppla, S. H.; Collier, R. J.; Liddington, R. C.; Cantley, L. C. The structural basis for substrate and inhibitor selectivity of the anthrax lethal factor. *Nat. Struct. Mol. Biol.* **2004**, *11*, 60–66.

(34) Xiong, Y.; Wiltsie, J.; Woods, A. G., J.; Pivnichny, J. V.; Tang, W.; Bansal, A.; Cummings, R. T.; Cunningham, B. R.; Friedlander, A. M.; Douglas, C. M.; Salowe, S. P.; Zaller, D. M.; Scolnick, E. M.; Schmatz, D. M.; Bartizal, K.; Hermes, J. D.; MacCoss, M.; Chapman, K. T. The discovery of a potent and selective lethal factor inhibitor for adjunct therapy of anthrax infection. *Bioorg. Med. Chem. Lett.* **2006**, *16*, 964–968.

(35) Konstantinopoulos, P. A.; Karamouzis, M. V.; Papatsoris, A. G.; Papavassiliou, A. G. Matrix metalloproteinase inhibitors as anticancer agents. *Int. J. Biochem. Cell Biol.* **2008**, *40*, 1156–1168.

(36) Levitt, N. C.; Eskens, F. A. L. M.; O'Byrne, K. J.; Propper, D. J.; Denis, L. J.; Owen, S. J.; Choi, L.; Foekens, J. A.; Wilner, S.; Wood, J. M.; Nakajima, M.; Talbot, D. C.; Steward, W. P.; Harris, A. L.; Verweij, J. Phase I and pharmacological study of the oral matrix metalloproteinase inhibitor, MMI1270 (CGS27023A), in patients with advanced solid cancer. *Clin. Cancer Res.* **2001**, *7*, 1912–1922.

(37) Andrianov, V.; Gailite, V.; Lola, D.; Loza, E.; Semenikhina, V.; Kalvinsh, I.; Finn, P.; Petersen, K. D.; Ritchie, J. W. A.; Khan, N.; Tumber, A.; Collins, L. S.; Vadlamudi, S. M.; Bjorkling, F.; Sehested, M. Novel amide derivatives as inhibitors of histone deacetylase: design, synthesis and SAR. *Eur. J. Med. Chem.* **2008**, doi:10.1016/j.ejmech.2008.06.020.

(38) Hajduk, P. J.; Sheppard, G.; Nettesheim, D. G.; Olejniczak, E. T.; Shuker, S. B.; Meadows, R. P.; Steinman, D. H.; Carrera, G. M., Jr.; Marcotte, P. A.; Severin, J.; Walter, K.; Smith, H.; Gubbins, E.; Simmer, R.; Holzman, T. F.; Morgan, D. W.; Davidsen, S. K.; Summers, J. B.; Fesik, S. W. Discovery of potent nonpeptide inhibitors of stromelysin using SAR by NMR. *J. Am. Chem. Soc.* **1997**, *119*, 5818–5827.

(39) Jacobsen, F. E.; Lewis, J. A.; Cohen, S. M. A new role for old ligands: discerning chelators for zinc metalloproteinases. *J. Am. Chem. Soc.* **2006**, *10*, 3156–3157.

(40) Lewis, J. A.; Mongan, J.; McCammon, J. A.; Cohen, S. M. Evaluation and binding-mode prediction of thiopyrone-based inhibitors of anthrax lethal factor. *ChemMedChem* **2006**, *7*, 694–697.

(41) Lewis, J. A.; Puerta, D. T.; Cohen, S. M. Metal complexes of the trans-influencing ligand thiomaltol. *Inorg. Chem.* **2003**, *42*, 7455–7459.

(42) Lewis, J. A.; Tran, B. L.; Puerta, D. T.; Rumberger, E. M.; Hendrickson, D. N.; Cohen, S. M. Synthesis, structure and spectroscopy of new thiopyrones and hydroxythiopyrone transition-metal complexes. *Dalton Trans.* **2005**, *15*, 2588–2596.

(43) Puerta, D. T.; Griffin, M. O.; Lewis, J. A.; Romero-Perez, D.; Garcia, R.; Villarreal, F. J.; Cohen, S. M. Heterocyclic zinc-binding groups for use in next generation matrix metalloproteinase inhibitors: potency, toxicity, and reactivity. *J. Biol. Inorg. Chem.* **2006**, *11*, 131–138.

(44) Puerta, D. T.; Lewis, J. A.; Cohen, S. M. New beginnings for matrix metalloproteinase inhibitors: identification of high-affinity zinc-binding groups. *J. Am. Chem. Soc.* **2004**, *126*, 8388–8389.

(45) Cummings, R. T.; Salowe, S. P.; Cunningham, B. R.; Wiltsie, J.; Park, Y. W.; Sonatore, L. M.; Wisniewski, D.; Douglas, C. M.; Hermes, J. D.; Scolnick, E. M. A peptide-based fluorescence resonance energy transfer assay for *Bacillus anthracis* lethal factor protease. *Proc. Natl. Acad. Sci. U.S.A.* **2002**, *99*, 6603–6606.

(46) Agrawal, A.; Romero-Perez, D.; Jacobsen, J. A.; Villarreal, F. J.; Cohen, S. M. Zinc-binding groups modulate selective inhibition of MMPs. *ChemMedChem* **2008**, *3*, 812–820.

(47) Abu-Dari, K.; Raymond, K. N. Ferric ion sequestering agents. 23. Synthesis of tris(hydroxypyridinethione) ligands and their ferric complexes; X-ray structure analysis of *N*,*N*′,*N*″-tris((1,2-didehydro-1-hydroxy-2-thioxopyrid-6-yl)carbonyl-2,2′,2′-triamino-triethylaminato)iron(III). *Inorg. Chem.* **1991**, *30*, 519–524.

(48) Scarrow, R. C.; Riley, P. E.; Abu-Dari, K.; White, D. L.; Raymond, K. N. Ferric ion sequestering agents. 13. Synthesis, structures, and thermodynamics of complexation of cobalt(III) and iron(III) tris complexes of several chelating hydroxypyridinones. *Inorg. Chem.* **1985**, *24*, 954–967.

(49) Hopkins, A. L.; Groom, C. R.; Alex, A. Ligand efficiency: a useful metric for lead selection. *Drug Discovery Today* **2004**, *9*, 430–431.

(50) Reynolds, C. H.; Bembenek, S. D.; Tounge, B. A. The role of molecular size in ligand efficiency. *Bioorg. Med. Chem. Lett.* **2007**, *17*, 4258–4261.

(51) Reynolds, C. H.; Tounge, B. A.; Bembenek, S. D. Ligand binding efficiency: trends, physical basis, and implications. *J. Med. Chem.* **2008**, *51*, 2432–2438.

(52) Morris, G. M.; Goodsell, D. S.; Halliday, R. S.; Huey, R.; Hart, W. E.; Belew, R. K.; Olson, A. J. Automated docking using a Lamarckian genetic algorithm and and empirical binding free energy function. *J. Comput. Chem.* **1998**, *19*, 1639–1662.

(53) Parkin, G. The bioinorganic chemistry of zinc: synthetic analogues of zinc enzymes that feature tripodal ligands. *Chem. Commun.* **2000**, *2000*, 1971–1985.

(54) Allen, F. H.; Bird, C. M.; Rowland, R. S.; Raithby, P. R. Resonance-induced hydrogen bonding at sulfur acceptors in $R_1R_2C{=}S$ and $R_1CS_2^-$ systems. *Acta Crystallogr.* **1997**, *B53*, 680–695.

(55) Hori, T.; Otani, Y.; Kawahata, M.; Yamaguchi, K.; Ohwada, T. Nonplanar structures of thioamides derived from 7-azabicyclo[2.2.1]heptane. Electronically tunable planarity of thioamides. *J. Org. Chem.* **2008**, *73*, 9102–9108.

(56) Pellecchia, M.; Bertini, I.; Cowburn, D.; Dalvit, C.; Giralt, E.; Jahnke, W.; James, T. L.; Homans, S. W.; Kessler, H.; Luchinat, C.; Meyer, B.; Oschkinat, H.; Peng, J.; Schwalbe, H.; Siegal, G. Perspectives on NMR in drug discovery: a technique comes of age. *Nat. Rev. Drug Discovery* **2008**, *7*, 738–745.

(57) Venkatesan, N.; Kim, B. H. Synthesis and enzyme inhibitory activities of novel peptide isosteres. *Curr. Med. Chem.* **2002**, *9*, 2243–2270.

(58) Hanzlik, R. P.; Vyas, K. P.; Traiger, G. J. Substituent effects on the hepatotoxicity of thiobenzamide derivatives in the rat. *Toxicol. Appl. Pharmacol.* **1978**, *46*, 685–694.

(59) Ikehata, K.; Duzhak, T. G.; Galeva, N. A.; Ji, T.; Koen, Y. M.; Hanzlik, R. P. Protein targets of reactive metabolites of thiobenzamide in rat liver in vivo. *Chem. Res. Toxicol.* **2008**, *21*, 1432–1442.

(60) Jeschke, P.; Harder, A.; Etzel, W.; Gau, W.; Thielking, G.; Bonse, G.; Iinuma, K. Synthesis and anthelmintic activity of thioamide analogues of cyclic octadepsipeptides such as PF1022A. *Pest Manage. Sci.* **2001**, *57*, 1000–1006.

(61) Pfund, E.; Lequeux, T.; Masson, S.; Vazeux, M.; Cordi, A.; Pierre, A.; Serre, V.; Herve, G. Efficient synthesis of fluorothiosparfosic acid analogues with potential antitumoral activity. *Bioorg. Med. Chem.* **2005**, *13*, 4921–4928.

(62) Sheldrick, G. M. S. *SHELXTL*, version 2.10; Bruker AXS, Inc.: Madison, WI, 2004. The semiempirical method used is based on a method of Blessing, R. H. *Acta Crystallogr*. **1995**, *A51*, 33.

(63) Case, D. A.; Perlman, D. A.; Caldwell, J. W.; Chetham, T. E., III; Ross, W. S.; Simmerling, C. L.; Darden, T. A.; Merz, K. M.; Stanton, R. V.; Cheng, A. L.; Vincent, J. J.; Crowley, M.; Tsui, V.; Gohlke, H.; Radmer, R. J.; Duan, Y.; Pitera, J.; Massova, I.; Seibel, G. L.; Singh, U. C.; Weiner, P. K.; Kollman, P. A. *AMBER*, version 7; University of California: San Francisco, CA, 2002.

(64) Cornell, W. D.; Cieplak, P.; Bayly, C. I.; Gould, I. R.; Merz, K. M.; Ferguson, D. M.; Spellmeyer, D. C.; Fox, T.; Caldwell, J. W.; Kollman, P. A. A 2nd generation force-field for the simulation of proteins, nucleic-acids, and organic-molecules. *J. Am. Chem. Soc.* **1995**, *117*, 5179–5197.

(65) Ryckaert, J. P.; Ciccotti, G.; Berendsen, H. J. C. Numerical-intergration of Cartesian equations of motion of a system with constraints, Molecular-dynamics of *N*-alkanes. *J. Comput. Phys.* **1977**, *23*, 327–341.

(66) Darden, T.; York, D.; Pedersen, L. Particle mesh Ewald, an $N\cdot\log(N)$ method for Ewald sums in large systems. *J. Chem. Phys.* **1993**, *98*, 10089–10092.

(67) Zhang, Y. K.; Liu, H. Y.; Yang, W. T. Free energy calculation on enzyme reactions with an efficient iterative procedure to determine minimum energy paths on a combined ab intio QM/MM potential energy surface. *J. Chem. Phys.* **2000**, *112*, 3483–3492.

(68) Liu, H. Y.; Zhang, Y. K.; Yang, W. T. How is the active site of enolase organized to catalyze two different reaction steps? *J. Am. Chem. Soc.* **2000**, *122*, 6560–6570.

(69) Zhang, Y. K.; Lee, T. S.; Yang, W. T. A pseudobond approach to combining quantum mechanical and molecular mechanical methods. *J. Chem. Phys.* **1999**, *110*, 46–54.

(70) Zhang, Y. K.; Kua, J.; McCammon, J. A. Role of the catalytic triad and oxyanion hole in acetylcholinesterase catalysis: an ab initio QM/MM study. *J. Am. Chem. Soc.* **2002**, *124*, 10572–10577.

(71) Cisneros, G. A.; Wang, M.; Silinski, P.; Fitzgerald, M. C.; Yang, W. T. The protein backbone makes important contributions to 4-oxalocrotonate tautomerase enzyme catalysis: understanding from theory and experiment. *Biochemistry* **2004**, *43*, 6885–6892.

(72) Cheng, Y. H.; Zhang, Y. K.; McCammon, J. A. How does the cAMP-dependent protein kinase catalyze the phosphorylation reaction: an ab intio QM/MM study. *J. Am. Chem. Soc.* **2005**, *127*, 1553–1562.

(73) Hu, P.; Zhang, Y. K. Catalytic mechanism and product specificity of the histone lysine methyltransferase SET7/9: An ab initio QM/MM-FE study with multiple initial structures. *J. Am. Chem. Soc.* **2006**, *128*, 1272–1278.

(74) Frisch, M. J.; Trucks, G. W.; Schlegel, H. B.; Scuseria, G. E.; Robb, M. A.; Cheeseman, J. R.; Zakrzewski, V. G.; Montgomery, J. A., Jr.; Stratmann, R. E.; Burant, J. C.; Dapprich, S.; Millam, J. M.; Daniels, A. D.; Kudin, K. N.; Strain, M. C.; Farkas, O.; Tomasi, J.; Barone, V.; Cossi, M.; Cammi, R.; Mennucci, B.; Pomelli, C.; Adamo, C.; Clifford, S.; Ochterski, J.; Petersson, G. A.; Ayala, P. Y.; Cui, Q.; Morokuma, K.; Malick, D. K.; Rabuck, A. D.; Raghavachari, K.; Foresman, J. B.; Cioslowski, J.; Ortiz, J. V.; Baboul, A. G.; Stefanov, B. B.; Liu, G.; Liashenko, A.; Piskorz, P.; Komaromi, I.; Gomperts, R.; Martin, R. L.; Fox, D. J.; Keith, T.; Al-Laham, M. A.; Peng, C. Y.; Nanayakkara, A.; Gonzalez, C.; Challacombe, M.; Gill, P. M. W.; Johnson, B.; Chen, W.; Wong, M. W.; Andres, J. L.; Head-Gordon, M.; Replogle, E. S.; Pople, J. A. *Gaussian 98*, revision A.5; Gaussian, Inc.: Pittsburgh, PA, 1998.

(75) Ponder, J. W. *TINKER, Software Tools for Molecular Design*, version 3.6; 1998.

(76) Amin, E. A.; Truhlar, D. G. Zn coordination chemistry: development of benchmark suites for geometries, dipole moments, and bond dissociation energies and their use to test and validate density functionals and molecular orbital theory. *J. Chem. Theory Comput.* **2008**, *4*, 75–85.

JM8013212